Analytical analysis of borehole experiments for the estimation of subsurface thermal properties

Luis G. Moscoso Lembcke[1,5], Delphine Roubinet[2,5], Floriane Gidel[1,3], James Irving[1], Peeter Pehme[4], and Beth L. Parker[4]

Abstract

Estimating subsurface thermal properties is required in many research fields and applications. To this end, borehole experiments such as the thermal response test (TRT) and active-line-source (ALS) method are of significant interest because they allow us to determine thermal property estimates *in situ*. With these methods, the subsurface thermal conductivity and diffusivity are typically estimated using asymptotic analytical expressions, whose simplifying assumptions have an impact on the accuracy of the values obtained. In this paper, we develop new analytical tools for interpreting borehole thermal experiments, and we use these tools to assess the impact of such assumptions on thermal property estimates. Quite importantly, our results show that the simplifying assumptions of currently used analytical models can result in errors in the estimated thermal conductivity and diffusivity of up to 60% and 40%, respectively. We also show that these errors are more

[1] Applied and Environmental Geophysics Group, University of Lausanne, Switzerland

[2] Corresponding author: delphine.roubinet@unil.ch; Applied and Environmental Geophysics Group, University of Lausanne, Switzerland

[3] Now at School of Mathematics, University of Leeds, United Kingdom

[4] G360 Centre for Applied Groundwater Research, University of Guelph, Canada

[5] These authors contributed equally to this work.

important for short-term analysis and can be reduced with an appropriate choice of experimental duration. Our results demonstrate the need for cautious interpretation of the data collected during TRT and ALS experiments as well as for improvement of the existing *in-situ* experimental methods.

Keywords: analytical solution, borehole experiments, thermal properties, *in-situ* estimation

1. Introduction

Accurate characterization and monitoring of heat transport in the subsurface is critically important in a wide variety of research fields and applications. In enhanced oil recovery and in the development of geothermal systems, for example, the transfer of heat between injected pore fluids and the host rock governs the effectiveness of the extraction procedures (e.g., (*Al-Hadhrami and Blunt*, 2001; *Gelet et al.*, 2012)). The presence of heat can also represent a significant risk for the environment as it can create or reopen microfractures (e.g., (*Lin*, 2002; *Wang et al.*, 1989)), which may have dramatic consequences such as seismic activity during geothermal exploitations (e.g., (*Chen and Shearer*, 2011; *Gunasekera et al.*, 2003)) and the leakage of nuclear waste (e.g., (*Wang et al.*, 1981; *Xiang and Zhang*, 2012)). Recently, heat transport has also gained significant interest for characterizing subsurface hydraulic properties and processes, since heat may be used as an effective groundwater tracer (*Anderson*, 2005; *Saar*, 2011; *Wagner et al.*, 2014). At the aquifer scale, temperature monitoring can help to quantify groundwater/surface-water interactions (e.g., (*Conant*, 2004; *Constantz*, 2008)) as well as to study groundwater discharge (e.g., (*Lowry et al.*, 2007)).

At the cross-borehole and borehole scales, heat has been used to determine subsurface structural heterogeneity, most notably the presence of fractures and their hydraulic characteristics (e.g., *Pehme et al.* (2013, 2014); *Coleman et al.* (2015)), and to quantify borehole vertical flows related to hydraulic experiments (e.g., *Klepikova et al.* (2011, 2014); *Read et al.* (2013)). Finally, at the lysimeter scale, examining temperature variations under forced thermal conditions can be used to estimate soil-moisture profiles (e.g., (*Ciocca et al.*, 2012; *Weiss*, 2003)).

For all of the above-mentioned applications, proper quantification of the subsurface thermal conductivity, as well as the thermal diffusivity when transient behavior is being considered, are of paramount importance because these material properties control the flow of heat in natural environments. Although property values for various rocks and soils may clearly be found in reference tables (e.g., (*Eppelbaum*, 2014)) or estimated from laboratory analyses of field samples (e.g., (*Jorand et al.*, 2013; *Popov et al.*, 1999)), there is no substitute for *in-situ* measurements when we require accurate estimates that are truly representative of natural conditions. To this end, two important borehole experiments that may be used to estimate subsurface thermal properties *in situ* are the thermal response test (TRT) and the active line source (ALS) method (Figure 1). With the standard TRT approach, heated water flows in a U-tube located in a borehole and the temperature is monitored at the inlet and outlet of the system over the course of heating, and commonly after heating has stopped. This method is widely used in geothermal studies in which thermal property estimates are required to evaluate the cost and efficiency of ground heat exchanger systems (e.g., *Lamarche et al.* (2010);

Rainieri et al. (2011); *Raymond et al.* (2011a)). With the ALS method, a heating cable is used to warm the water in the borehole and the temperature is recorded as a function of time at one or a variety of locations along the borehole. The latter can be done via borehole logging using a dedicated temperature probe (e.g., *Pehme et al.* (2007)) or using distributed temperature sensing (DTS) technology (e.g., *Coleman et al.* (2015)). Here, applications to date have been in hydrogeology where the primary aim has been to identify hydraulically-active fractures by studying the variation of thermal properties along the borehole using, in most cases, a flexible fabric liner in order to avoid hydraulic connections through the borehole (e.g., *Pehme et al.* (2013); *Coleman et al.* (2015)). Note that recent work with TRT experiments has also involved active heating without the use of flowing water (*Raymond and Lamarche*, 2014; *Raymond et al.*, 2015).

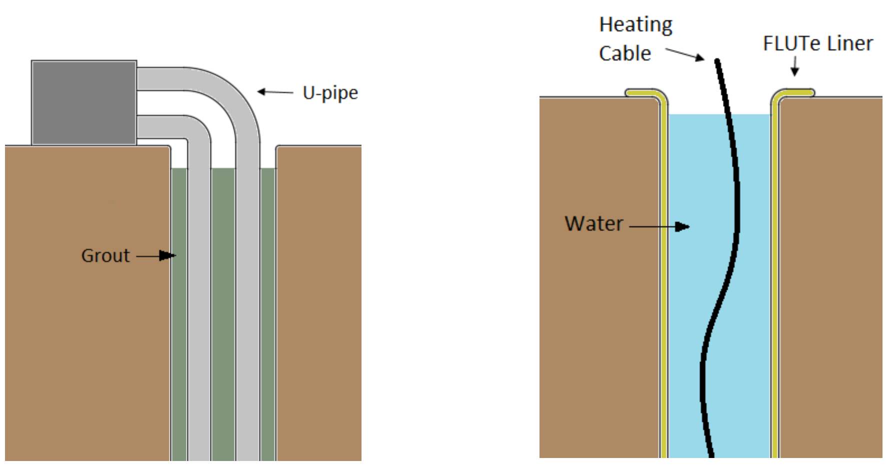

(a) Thermal response test (b) Active line source method

Figure 1: Borehole thermal experiments considered in this study to evaluate subsurface thermal properties *in situ*.

Typically, the estimation of subsurface thermal properties from TRT and ALS measurements has relied upon asymptotic analytical expressions describing the temperature variation at the borehole wall in response to a line heat source (e.g., *Esen and Inalli* (2009); *Hu et al.* (2012); *Pehme et al.* (2013); *Raymond et al.* (2011a)). For ALS measurements, these expressions are used directly with the measured data, whereas TRT measurements require the addition of an equivalent resistance model in order to relate the borehole-wall and monitored temperatures (e.g., *Raymond et al.* (2011a)). The strong advantage of asymptotic solutions in this context is that they provide relatively simple time-domain analytical expressions that permit easy and rapid interpretation of the acquired temperature data. Indeed, the slope of these solutions is proportional to the inverse of the matrix thermal conductivity, whereas the y-intercept can be related to the matrix thermal diffusivity. A key drawback of the asymptotic expressions considered to date, however, is that they are based upon assumptions that, although greatly facilitating the mathematical development, cannot be considered as realistic for a wide range of practical scenarios. Most notably, currently used asymptotic solutions for interpreting TRT and ALS experiments are derived from analytical solutions that either (i) consider the borehole thermal properties to be the same as those of the matrix, meaning that the heat source is assumed to be embedded within the host rock (e.g., (*Eskilson*, 1987)); or (ii) assume that the heat source is located exactly at the borehole center (e.g., (*Beck et al.*, 1971; *Shen and Beck*, 1986)). Clearly, violation of these assumptions may have an effect on the thermal property estimates obtained from TRT and ALS data. Related to this, the time after heating for which the asymptotic solutions are valid, commonly referred to as the "asymptotic time" and assumed to occur after only a few hours, depends upon these assumptions being upheld, which implies that significant errors could be expected when interpreting short-term experiments. Note that, although some work has been done to develop better full solutions for the borehole temperature that take into account the presence of the borehole (e.g., (*Lamarche and Beauchamp*, 2007a; *Hu et al.*, 2012; *Bozzoli et al.*, 2011; *Raymond et al.*, 2011)), the assumption of the heat source located directly at the borehole center is always made.

In this paper, in an attempt to address the above issues, we present new analytical solutions for interpreting TRT and ALS experiments that account for the borehole thermal properties and are completely flexible with respect to the location of the heat source in the borehole. These analytical expressions are derived in the Laplace domain and fully describe the short- and long-term variation of temperature anywhere in the borehole. From these solutions, we also derive simplified asymptotic analytical expressions in the time domain that can be used for accurate and easy interpretation of TRT and ALS experimental data. We choose an analytical rather than numerical approach for this work because analytical solutions help to improve our understanding of the problem, most notably for identifying what experimental parameters and model properties have the largest impact on the measured temperature data, as well as determining what experimental configurations will offer the most accurate estimates of thermal properties. Further, the low computational cost of analytical solutions is ideal for performing detailed parameter sensitivity analyses and stochastic uncertainty assessment, both of which can require hundreds if not thousands of model computations.

We begin by formulating an expression for the spatial and temporal distribution of temperature in a general borehole-matrix system subject to a line-source heat injection in the borehole (Section 2). Next, we use this result to derive specific expressions for interpreting ALS and TRT experiments, which are validated against numerical and existing analytical solutions (Section 3). Finally, the developed expressions are used to assess (i) the range of validity of standard asymptotic solutions; (ii) the potential for errors in subsurface thermal property estimates resulting from the use of these solutions; and (iii) what experimental configurations can reduce the impact of the assumptions related to these solutions on the accuracy of thermal property estimates (Section 4).

2. General solution for temperature in a borehole-matrix system subject to a line heat source

We develop below new analytical expressions for temperature in a borehole-matrix system considering a line-source heat injection located somewhere within the borehole. As is the case with all previous work in this domain (e.g., (*Lamarche et al.*, 2010; *Raymond et al.*, 2011a)), vertical flow in the borehole and convection in the formation are not considered in our analysis as they are expected to be minimal for the case of lined or cased boreholes. The results, presented in the Laplace domain and in terms of dimensionless quantities, are then used in Section 3 to develop full and asymptotic analytical expressions, in the Laplace and time domains respectively, for interpreting ALS and TRT experiments.

2.1. Problem formulation

Figure 2 shows a general borehole-matrix system in cross-section where R [m] is the borehole radius, K [W/(m·°C)] is the thermal conductivity, d [kg/m^3] is the density, and c [J/(kg·°C)] is the specific heat capacity. Subscripts 1 and 2 refer to the borehole and matrix domains, respectively, which are defined in polar coordinates by $\Omega_b = \{(r, \theta) : 0 \leq r \leq R, 0^\circ \leq \theta < 360^\circ\}$ and $\Omega_m = \{(r, \theta) : R \leq r < \infty, 0^\circ \leq \theta < 360^\circ\}$. Considering the presence of a line heat source $q(r, \theta, t)$ [W/m^3] somewhere within Ω_b, the temperature $T_1(r, \theta, t)$ [°C] in the borehole satisfies the heat equation

$$\frac{\partial T_1}{\partial t} - \alpha_1 \frac{\partial^2 T_1}{\partial r^2} - \frac{\alpha_1}{r}\frac{\partial T_1}{\partial r} - \frac{\alpha_1}{r^2}\frac{\partial^2 T_1}{\partial \theta^2} = \frac{q}{d_1 c_1}, \qquad (r, \theta) \in \Omega_b. \tag{1a}$$

Similarly, the temperature $T_2(r, \theta, t)$ in the matrix satisfies

$$\frac{\partial T_2}{\partial t} - \alpha_2 \frac{\partial^2 T_2}{\partial r^2} - \frac{\alpha_2}{r}\frac{\partial T_2}{\partial r} - \frac{\alpha_2}{r^2}\frac{\partial^2 T_2}{\partial \theta^2} = 0, \quad (r, \theta) \in \Omega_m, \tag{1b}$$

where the thermal diffusivity $\alpha_i = K_i/(d_i c_i)$. For a heat injection of Q [W/m] at position (r^*, θ^*) from time $t = 0$ to t^*, the source term q in equation (1a) is defined as

$$q(r, \theta, t) = Qu(t^* - t)\delta(r - r^*, \theta - \theta^*)/r, \tag{2}$$

where $u(.)$ is the Heaviside step function and $\delta(.)$ is the Dirac delta function.

Equations (1) are subject to (i) the initial conditions

$$T_1(r, \theta, 0) = T^0(r, \theta), \quad T_2(r, \theta, 0) = T^0(r, \theta), \tag{3a}$$

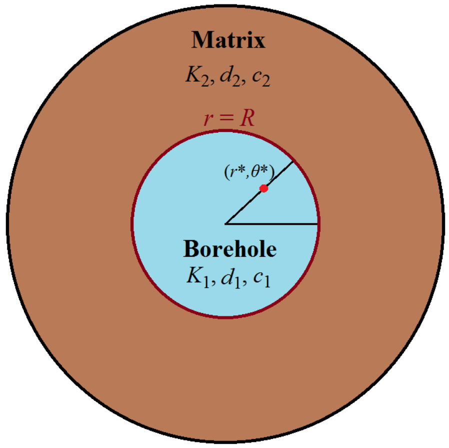

Figure 2: Cross section of a general borehole-matrix system in polar coordinates. A line heat source is located at position (r^*, θ^*) inside the borehole.

where $T^0(r, \theta)$ is the initial temperature in the system; (ii) the boundary conditions

$$T_1(r \to 0, \theta, t) < \infty, \quad T_2(r \to \infty, \theta, t) = T^0(r \to \infty, \theta); \tag{3b}$$

and (iii) the continuity conditions at the borehole-matrix interface where $r = R$

$$T_1 = T_2, \quad K_1 \frac{\partial T_1}{\partial r} = K_2 \frac{\partial T_2}{\partial r}. \tag{3c}$$

Defining the dimensionless parameters $\mathcal{T}_i$ $(i = 1, 2)$, τ, ρ, κ, and a as

$$\mathcal{T}_i = \frac{T_i}{Q/K_1}, \quad \tau = \frac{t}{R^2/\alpha_1}, \quad \rho = r/R, \tag{4}$$

$$\kappa = K_2/K_1, \quad a = \alpha_2/\alpha_1,$$

expressions (1) can be rewritten as

$$\frac{\partial \mathcal{T}_1}{\partial \tau} - \frac{\partial^2 \mathcal{T}_1}{\partial \rho^2} - \frac{1}{\rho}\frac{\partial \mathcal{T}_1}{\partial \rho} - \frac{1}{\rho^2}\frac{\partial^2 \mathcal{T}_1}{\partial \theta^2} = \lambda, \quad (\rho, \theta) \in \tilde{\Omega}_b, \tag{5a}$$

with $\lambda = \delta(\rho - \rho^*, \theta - \theta^*) u(\tau^* - \tau)/\rho$, and

$$\frac{\partial \mathcal{T}_2}{\partial \tau} - a\frac{\partial^2 \mathcal{T}_2}{\partial \rho^2} - \frac{a}{\rho}\frac{\partial \mathcal{T}_2}{\partial \rho} - \frac{a}{\rho^2}\frac{\partial^2 \mathcal{T}_2}{\partial \theta^2} = 0, \quad (\rho, \theta) \in \tilde{\Omega}_m, \tag{5b}$$

where the borehole and matrix domains in terms of the dimensionless parameters are now defined by $\tilde{\Omega}_b = \{(\rho, \theta) : 0 \leq \rho \leq 1, 0^\circ \leq \theta < 360^\circ\}$ and $\tilde{\Omega}_m = \{(\rho, \theta) : 1 \leq \rho < \infty, 0^\circ \leq \theta < 360^\circ\}$, respectively. Conditions (3) can then be rewritten as

$$\mathcal{T}_1(\rho, \theta, 0) = \mathcal{T}^0(\rho, \theta), \quad \mathcal{T}_2(\rho, \theta, 0) = \mathcal{T}^0(\rho, \theta), \tag{6a}$$

$$\mathcal{T}_1(\rho \to 0, \theta, \tau) < \infty, \quad \mathcal{T}_2(\rho \to \infty, \theta, \tau) = \mathcal{T}^0(\rho \to \infty, \theta), \tag{6b}$$

$$\mathcal{T}_1 = \mathcal{T}_2, \quad \frac{\partial \mathcal{T}_1}{\partial \rho} = \kappa \frac{\partial \mathcal{T}_2}{\partial \rho} \equiv g, \quad \rho = 1, \tag{6c}$$

where $\mathcal{T}^0$ is the initial dimensionless temperature defined as $\mathcal{T}^0 = T^0 K_1/Q$, and $g(\theta, \tau)$ is the (unknown) dimensionless thermal flux between the borehole and matrix domains.

In order to simplify the mathematical development, note that evaluating $\mathcal{T}_1$ and $\mathcal{T}_2$ with initial condition (6a) is equivalent to evaluating $\mathcal{T}_1 - \mathcal{T}^0$ and $\mathcal{T}_2 - \mathcal{T}^0$ with the initial dimensionless temperature set to zero. In the following, we thus consider $\mathcal{T}^0 = 0$ with $\mathcal{T}_1$ and $\mathcal{T}_2$ representing the difference between the current and initial dimensionless temperatures.

2.2. Laplace-domain analytical expressions

To determine general Laplace-domain analytical expressions for the dimensionless temperature in the borehole and matrix domains satisfying equations (5) and (6), we consider a two-step coupling approach involving domain-specific Green's functions (e.g., (*Roubinet et al.*, 2012; *Ruiz Martinez et al.*, 2014)). In the first step of this approach, initial conditions (6a), boundary conditions (6b), and only the second continuity condition (6c) are used to formulate integral expressions for $\mathcal{T}_1$ and $\mathcal{T}_2$ in terms of the Green's functions $\mathcal{T}_1^*(\rho,\rho',\theta,\theta',\tau,\tau')$ and $\mathcal{T}_2^*(\rho,\rho',\theta,\theta',\tau,\tau')$. Derivation of the latter functions can be found in Appendices A.1 and A.2, respectively, whereas details of the integral formulation are presented in Appendix B.1. The result is

$$\mathcal{T}_1(\rho,\theta,\tau) = \int_0^\tau u(\tau^*-\tau')\mathcal{T}^*_{1\,|\rho'=\rho^*,\theta'=\theta^*}\mathrm{d}\tau' + \int_0^\tau\int_0^{2\pi} g(\theta',\tau')\mathcal{T}^*_{1\,|\rho'=1}\mathrm{d}\theta'\mathrm{d}\tau' \tag{7a}$$

and

$$\mathcal{T}_2(\rho,\theta,\tau) = -\frac{a}{\kappa}\int_0^\tau\int_0^{2\pi} g(\theta',\tau')\mathcal{T}^*_{2\,|\rho'=1}\mathrm{d}\theta'\mathrm{d}\tau'. \tag{7b}$$

In the second step, we determine the Laplace transforms of $\mathcal{T}_1(\rho,\theta,\tau)$ and $\mathcal{T}_2(\rho,\theta,\tau)$ by considering the first continuity condition (6c). The corresponding details can be found in Appendix B.2, yielding

$$\bar{\mathcal{T}}_1(\rho,\theta,s) = \begin{cases} A(s)\omega_1 + 2A(s)S_1, & \rho<\rho^*,\\ A(s)\omega_2 + 2A(s)S_2, & \rho>\rho^*,\end{cases} \tag{8a}$$

and

$$\bar{\mathcal{T}}_2(\rho,\theta,s) = A(s)\omega_3 + 2A(s)S_3, \tag{8b}$$

where

$$\omega_1 = I_0(q_1\rho)H_0(\rho^*), \tag{9a}$$

$$\omega_2 = I_0(q_1\rho^*)H_0(\rho), \tag{9b}$$

$$\omega_3 = I_0(q_1\rho^*)\frac{K_0(q_2\rho)}{K_0(q_2)h_0}, \tag{9c}$$

$$S_1 = \sum_{m=1}^{\infty} I_m(q_1\rho)H_m(\rho^*)\cos\left[m(\theta-\theta^*)\right], \tag{9d}$$

$$S_2 = \sum_{m=1}^{\infty} I_m(q_1\rho^*)H_m(\rho)\cos\left[m(\theta-\theta^*)\right], \tag{9e}$$

and

$$S_3 = \sum_{m=1}^{\infty} I_m(q_1\rho^*)\frac{K_m(q_2\rho)}{K_m(q_2)}h_m\cos\left[m(\theta-\theta^*)\right]. \tag{9f}$$

Here, $A(s) = (1-e^{-s\tau^*})/(2\pi s)$, quantities $I_m(.)$, $K_m(.)$, q_1, and q_2 are defined in Appendix A, and quantities $H_m(.)$ and h_m are defined in Appendix B.2.

3. Temperature expressions for borehole thermal experiments

We now show how the general Laplace-domain expression for temperature in the borehole given by equation (8a) can be directly utilized to fully model ALS experiments, and as a starting point in the development of a full temperature solution for TRT experiments. Again, this represents a substantial improvement compared to previous work in that (i) we allow for the heat source to be located anywhere within the borehole; and (ii) the borehole thermal properties are taken into account. Corresponding asymptotic time-domain analytical expressions are also derived for convenient and rapid interpretation of borehole temperature data.

3.1. Active line source (ALS) experiments

For ALS experiments, expression (8a) represents an exact solution in the Laplace domain for the dimensionless temperature monitored at position (ρ, θ) in the borehole corresponding to a heat source at position (ρ^*, θ^*) from time $\tau = 0$ to τ^*. The expression is valid for all times after heating begins and therefore describes fully the ALS experiment, but it cannot be inverted analytically for a corresponding time-domain formulation. Indeed, in order to use expression (8a) for the interpretation of ALS data, a numerical inverse Laplace transform is required. However, it is possible to derive a time-domain analytical expression for the asymptotic behavior of equation (8a) by (i) rewriting the full solution $\bar{\mathcal{T}}_1$ in terms of a reduced solution corresponding to a heat source from $\tau = 0$ to ∞; and (ii) deriving a time-domain asymptotic expression for this reduced solution through an analytical inverse Laplace transform. The corresponding derivation can be found in Appendix C.1, with the following result:

$$\mathcal{T}_1^{\infty} = \mathcal{T}_1^{h,\infty}(\rho, \theta, \tau) - u(\tau - \tau^*)\, \mathcal{T}_1^{h,\infty}(\rho, \theta, \tau - \tau^*), \tag{10}$$

where $\mathcal{T}_1^{h,\infty}$ is the reduced solution

$$\begin{aligned} \mathcal{T}_1^{h,\infty}(\rho, \theta, \tau) = {} & \frac{1}{4\pi\kappa}\left[\ln(\tau) + \ln(4a) - \gamma\right] \\ & - \frac{1}{4\pi}\left\{\ln\left(D^2\right) - \frac{\kappa - 1}{\kappa + 1}\ln\left[D^2 + \left(1 - \rho^{*2}\right)\left(1 - \rho^2\right)\right]\right\}. \end{aligned} \tag{11}$$

Here, γ is the EulerMascheroni constant and $D = \sqrt{\rho^{*2} - 2\rho\rho^* \cos(\theta - \theta^*) + \rho^2}$ is the dimensionless distance between the temperature sensor and the heat source. Note that when $\rho = 1$, $\theta = 0°$, $\rho^* = 0$, and $a = 1$, expression (11) reduces to the standard line-source model developed by *Carslaw and Jaeger*

(1986) where the distance between the observed temperature and heat source is equal to the borehole radius and the borehole properties are ignored.

To validate the full and asymptotic solutions (8a) and (10), respectively, we consider an ALS measurement configuration where the temperature is monitored at the borehole wall and the heat source is located at an off-center position inside the borehole (Figure 3). Table 1 shows the borehole and matrix properties that were assumed, which correspond to water and granite, respectively (*Carslaw and Jaeger*, 1986). Figure 4 shows the temperature results computed with these solutions, along with those obtained using the COMSOL Multiphysics finite-element software package. Note that the Stehfest algorithm (*Stehfest*, 1970) was used to transform the Laplace-domain results of equation (8a) into the time domain, which makes our implementation of this equation semi-analytical. The good agreement observed in Figure 4a between our results and the finite-element calculation validates the developed analytical solutions. As expected, we see that our asymptotic solution (10) has limited ability to model the temperature behavior during the early phases of heating and cooling (Figure 4b and 4c).

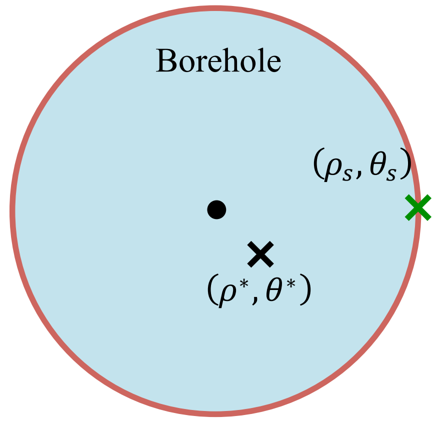

Figure 3: Configuration used to validate expressions (8a) and (10) for the monitored temperature during ALS experiments. The temperature sensor coordinates are defined as $\rho_s = 1$ and $\theta_s = 0°$ (green cross), and the heat source coordinates as $\rho^* = 0.3$ and $\theta^* = -45°$ (black cross). The borehole center is indicated with a black circle.

Table 1: Borehole and matrix properties used for validating temperature expressions (8a) and (10) for ALS experiments.

	Borehole ($i = 1$)	Matrix ($i = 2$)
Radius, R [m]	0.05	-
Thermal conductivity, K_i [W/(m·°C)]	0.61	2.51
Thermal diffusivity, α_i [m^2/s]	1.46×10^{-7}	1.2×10^{-6}
Heat source, Q [W/m]	15	-

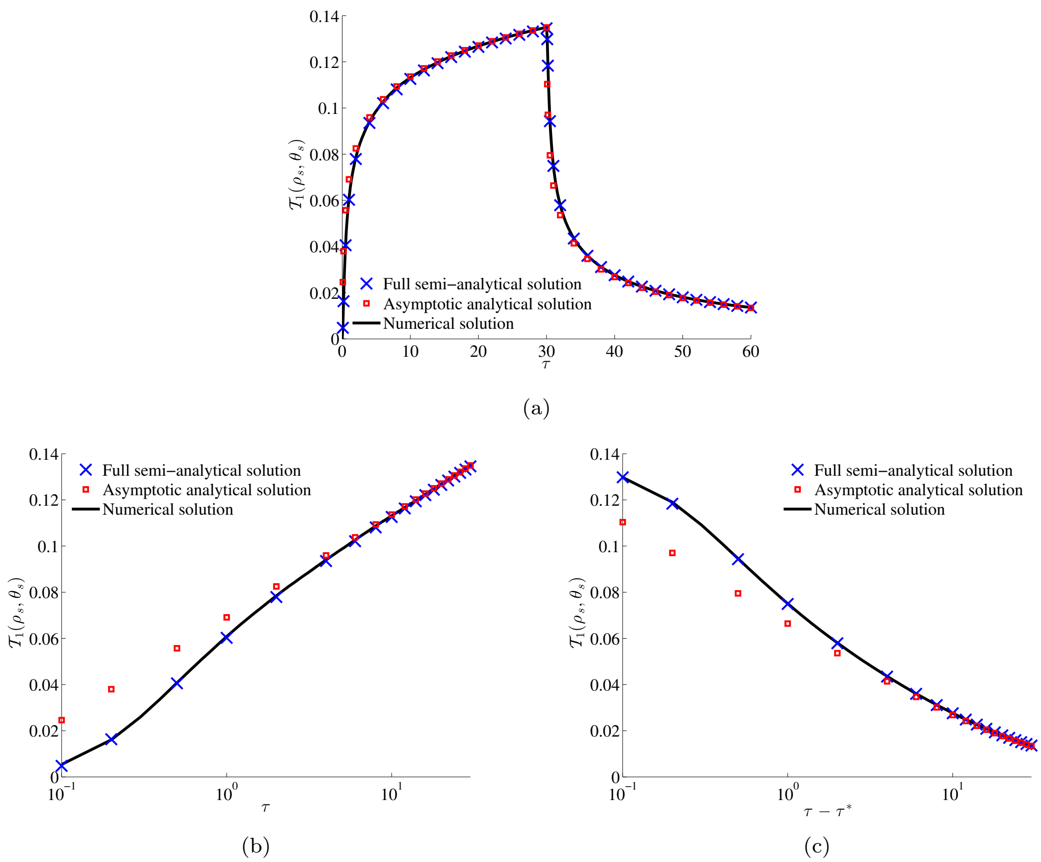

Figure 4: Dimensionless temperature at the sensor position for the configuration illustrated in Figure 3. The temperature is plotted as a function of (a) dimensionless time τ for the entire experiment; (b) dimensionless time τ for the heating period ($\tau < \tau^*$); and (c) dimensionless time $\tau - \tau^*$ for the cooling period ($\tau > \tau^*$). The dimensionless times are represented using (a) a linear scale, and (b-c) a logarithmic scale. Shown are the results of our full solution (8a) (blue crosses), our asymptotic solution (10) (red squares), and a reference finite-element numerical solution (black line).

3.2. Thermal response test (TRT) method

As mentioned previously, standard TRT experiments involve the flow of heated water through a U-pipe located in a borehole. The temperature of the water is monitored at the two extremities of the pipe and typically the average of these two temperatures is used to estimate the subsurface thermal properties (e.g., (*Lamarche et al.*, 2010; *Raymond et al.*, 2011a)). Below, we use T_f^i $(i = 1, 2)$ to denote the water temperature monitored at extremity i of the U-pipe and T_{TRT} to denote the average temperature. Normally, an analytical expression for T_{TRT} is obtained by considering the cross-section of the U-pipe in the borehole and representing it as a two-pipe system (Figure 5a). For each segment i of the pipe, an expression for T_f^i can be derived by: (i) writing T_f^i as a function of the temperature averaged over the external surface of the pipe, T_p^i, using an equivalent pipe thermal resistance model (Figure 5b-c); and (ii) writing T_p^i as a function of the borehole-wall temperature using a line-source model associated with an equivalent borehole resistance model (e.g., (*Lamarche et al.*, 2010; *Raymond et al.*, 2011a)). This borehole resistance model permits taking into account the borehole thermal properties that are not considered in standard line-source models, and it relies on an effective representation of these properties through a resistance parameter that is evaluated from the data collected during the TRT experiment.

In the present study, we wish to derive an expression for T_{TRT} using the results of Section 2. To this end, we develop a new solution for the temperature T_p^i on the external surface of pipe i considering the presence of heated water in the two pipes of the system. As our work explicitly takes

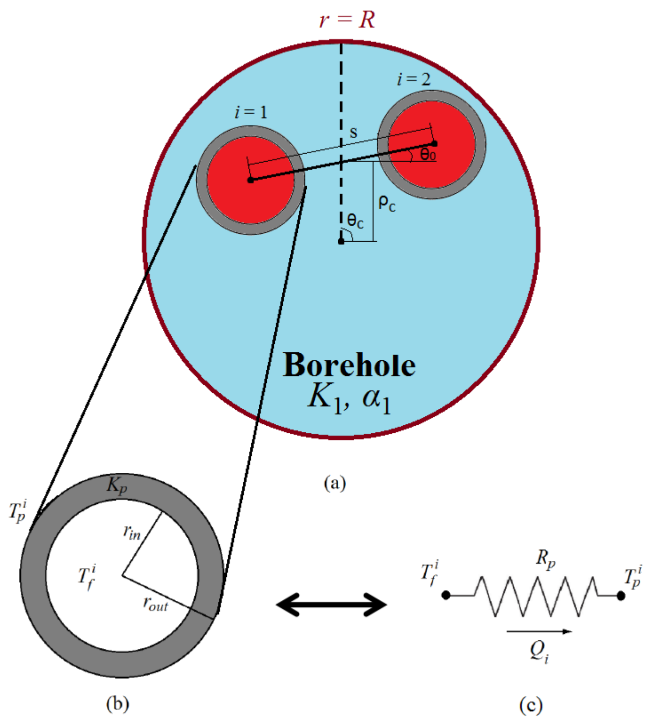

Figure 5: (a) Cross-sectional view of a U-pipe inside a borehole of radius R having thermal properties K_1 and α_1. (b) Zoom showing the details of the pipe where K_p is its thermal conductivity, and r_{in} and r_{out} are its inner and outer radii, respectively. (c) Equivalent pipe thermal resistance model using resistance R_p and heat flux Q_i.

into account the borehole thermal properties, T_p^i can be expressed without the need for an equivalent borehole resistance model as described above. In particular, it can be obtained by superposing temperatures $T_p^{i,1}$ and $T_p^{i,2}$, which are defined as the temperatures averaged over the external surface of pipe i considering a source term at pipe 1 and pipe 2, respectively. Appendix C.2 contains the corresponding derivation, as well as the derivation of the full solution for T_{TRT} and its dimensionless equivalent $\mathcal{T}_{TRT}$. The latter is valid for any position of the U-pipe in the borehole, and given by

$$\mathcal{T}_{TRT} =(Q_1\mathcal{T}_p^{av,1} + Q_2\mathcal{T}_p^{av,2})/(Q_1 + Q_2) + R_p K_1/2, \tag{12}$$

where Q_i is the heat flux from the fluid to the external surface of pipe i, and $\mathcal{T}_p^{av,j}$ is the average of dimensionless temperatures $\mathcal{T}_p^{1,j}$ and $\mathcal{T}_p^{2,j}$, given by $\mathcal{T}_p^{i,j} = K_1 T_p^{i,j}/Q_j$ $(i = 1, 2)$.

Equation (12) requires the numerical computation of an integral and an inverse Laplace transform in order to express $\mathcal{T}_{TRT}$ in the time domain, and thus its implementation is semi-analytical. As before, we therefore derive a corresponding asymptotic analytical time-domain expression $\mathcal{T}_{TRT}^{\infty}$, which assumes that the U-pipe is located at the borehole center. The corresponding derivation can be found in Appendix C.2, with the following result:

$$\begin{aligned}\mathcal{T}_{TRT}^{\infty} =& \frac{1}{4\pi\kappa}\left[\ln(\tau) + \ln(4a) - \gamma\right] \\ &+ \frac{1}{4\pi}\left[-\ln\left(D_1\rho_{out}\right) + \frac{\kappa-1}{\kappa+1}\ln\left(D_2\right) + \frac{1}{\kappa_p}\ln\left(\frac{\rho_{out}}{\rho_{in}}\right)\right],\end{aligned} \tag{13}$$

where $\kappa_p = K_p/K_1$, $D_1 = s/R$ with s the distance between the two pipes, $D_2 = 1 - {D_1}^4/16$, and ρ_{in} and ρ_{out} are the dimensionless inner and outer radii of the pipes, respectively.

To validate expressions (12) and (13), we consider two configurations where the U-pipe is located at different positions within the borehole. As illustrated in Figure 5a, its position is defined by the coordinates (ρ_c, θ_c) of its center, and the angle θ_0 of pipe 2 with respect to the horizontal line passing through the center of the U-pipe, where pipe 2 is the pipe with the warmest monitored temperature (i.e., $T_f^2 > T_f^1$). Tables 2 and 3 show the borehole, matrix, and U-pipe properties that were assumed for the validation where the borehole is considered to be filled with grout (*Raymond et al.*, 2011b). In the first configuration (Figure 6a), the U-pipe is located at an off-center position inside the borehole. Figure 7a shows the corresponding data computed using our full solution (12) and the COMSOL Multiphysics finite-element software. The good agreement observed between these two curves demonstrates the validity of the full solution. In the second configuration (Figure 6b), the U-pipe is centered in the borehole. Figure 7b shows the corresponding data computed using our asymptotic solution (13), COMSOL, and the borehole resistance model developed by *Raymond et al.* (2011b). As before, the finite-element solution is used for validation, whereas the borehole resistance model is used for comparison with existing models that are often used for interpreting TRT experiments. Figure 7b shows an acceptable agreement between all three curves with some small discrepancies observed at the beginning of the heating ($\tau \simeq 0$) and cooling ($\tau \simeq 11$) periods. These differences result from the limited ability of our asymptotic solution and the borehole resistance model to accurately reproduce short-term temperature measurements. However, in comparison with the borehole resistance model, the explicit representation of the borehole thermal properties used in our solutions avoids the need for an extra parameter, usually referred to as the borehole thermal resistance, that must be estimated from *in-situ* experimental data.

Table 2: Properties of the borehole-matrix system used for validating temperature expressions (12) and (13) for TRT experiments.

	Borehole ($i = 1$)	Matrix ($i = 2$)
Radius, R [m]	0.076	-
Thermal conductivity, K_i [W/(m·°C)]	1.2	2.51
Thermal diffusivity, α_i [m^2/s]	3.53×10^{-7}	1.02×10^{-6}
Initial temperature, T^0 [°C]	10	10

Table 3: Properties of the U-pipe system used for validating temperature expressions (12) and (13) for TRT experiments.

Inner radius, r_{in} [m]	0.017
Outer radius, r_{out} [m]	0.021
Pipe spacing, s [m]	0.07
Thermal conductivity, K_p [W/(m·°C)]	0.4
Heat source, Q_1 [W/m]	30
Heat source, Q_2 [W/m]	20
Heating time, t^* [h]	50

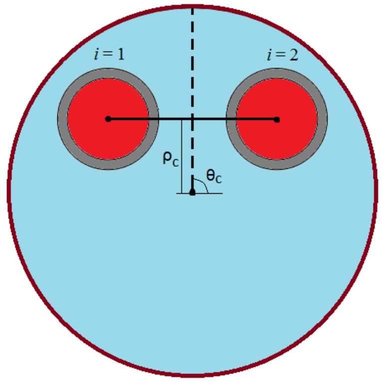

(a)

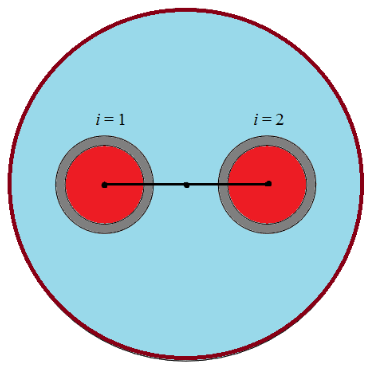

(b)

Figure 6: Configurations used to validate expressions (12) and (13) for the monitored temperature during TRT experiments. The U-pipe center is located at (a) the dimensionless distance $\rho_c = 0.3$ from the borehole center, and (b) the borehole center. In each case, $\theta_c = 90°$ and $\theta_0 = 0°$.

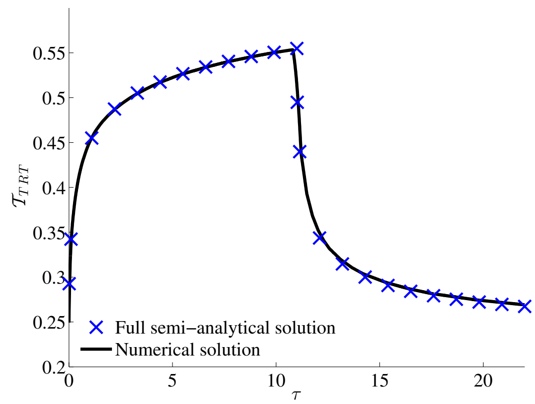

(a)

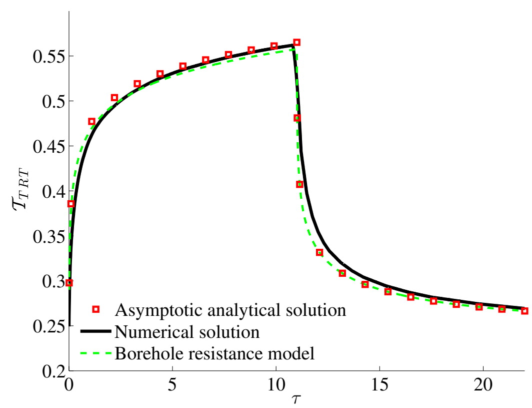

(b)

Figure 7: Dimensionless temperature for TRT experiments as a function of dimensionless time τ. (a) Full solution (12) (blue crosses) and finite-element numerical solution (black line) for the configuration in Figure 6a. (b) Asymptotic solution (13) (red squares), finite-element numerical solution (black line), and results obtained using the borehole resistance model of *Raymond et al.* (2011b) (dashed green line) for the configuration in Figure 6b.

3.3. Comments on the heating and cooling periods

ALS and TRT experiments are characterized by heating and cooling periods that can both be used to evaluate subsurface thermal properties. To understand if one of these periods is more suitable than the other for this purpose, we write expression (C.1) in the time domain, which leads to the following expression for $\mathcal{T}_1$:

$$\mathcal{T}_1(\rho, \theta, \tau) = \mathcal{T}_1^h(\rho, \theta, \tau) - u(\tau - \tau^*)\mathcal{T}_1^h(\rho, \theta, \tau - \tau^*) \quad (14)$$

where $\mathcal{T}_1^h$ is the temperature solution corresponding to a heat source from $\tau = 0$ to ∞. Expression 14 can be rewritten as

$$\mathcal{T}_1(\rho, \theta, \tau) = \begin{cases} \mathcal{T}_1^h(\rho, \theta, \tau), & \tau < \tau^*, \\ \mathcal{T}_1^c(\rho, \theta, \tau), & \tau \geq \tau^*, \end{cases} \quad (15)$$

where $\mathcal{T}_1^c$ is the temperature during the cooling period given by

$$\mathcal{T}_1^c(\rho, \theta, \tau) = \mathcal{T}_1^h(\rho, \theta, \tau) - \mathcal{T}_1^h(\rho, \theta, \tau - \tau^*). \quad (16)$$

Equation (16) demonstrates that there is a symmetric behavior of the temperature during the heating and cooling periods, which is seen in Figures 4b and 4c for the case where $\tau^* = 30$. This means that the asymptotic solution will have the same limited ability to model the temperature behavior at early times during both heating and cooling. Consequently, the error in the estimated thermal properties related to the use of asymptotic solutions is assumed to be similar for the heating and cooling periods, and we consider that these periods are equally suitable to evaluate the thermal properties. For this reason, the following section on the error analysis of temperature curve used to estimate thermal properties only focuses on the heating period of the experiments, and similar results are assumed when using temperatures measured during the cooling period.

4. Error analysis

We next use the full and asymptotic expressions developed in Section 3 to investigate (i) the time ranges over which the asymptotic expressions are valid; (ii) the effect of erroneous assumptions regarding the borehole thermal properties and position of the heat source on estimates of the subsurface thermal conductivity and diffusivity; and (iii) which TRT and ALS measurement configurations will result in the most reliable estimates of these properties.

4.1. Determination of the asymptotic time

For times greater than the asymptotic time, there will be good agreement between the asymptotic and full temperature solutions and therefore the asymptotic solution can be considered to be a valid approximation. With standard line-source models, the asymptotic time is usually defined as

$$t_1^{st} = 5R^2/\alpha_2, \tag{17}$$

which is based on a maximum relative error between the exact and asymptotic solutions of 2% (e.g., (*Eskilson*, 1987; *Lamarche and Beauchamp*, 2007b; *Raymond et al.*, 2011a)). For typical borehole diameters, this corresponds to a time period between 2 and 6 hours, implying that temperature measurements acquired after this amount of time should be interpretable with asymptotic solutions. Note, however, that the above simple formula relies upon the assumptions of standard line-source models, which are not realized in many practical situations. Consequently, we examine here using our developed solutions the impact of the borehole thermal properties (Section 4.1.1) as well as the heat source position (Section 4.1.2) on the dimensionless asymptotic time τ_1, and we compare these results to those obtained using the standard assumptions. In particular, we evaluate τ_1 at the borehole wall considering a single heat source term using equation (8a), as expressions derived for both ALS and TRT experiments usually rely upon this temperature.

4.1.1. Impact of the borehole thermal properties

The relative error E_1 between the exact and asymptotic temperature solutions derived in Sections 2.2 and 3.1, respectively, can be defined as

$$E_1(\tau) = \left| \frac{\mathcal{T}_1 - \mathcal{T}_1^{\infty}}{\mathcal{T}_1} \right|, \tag{18}$$

where the exact solution $\mathcal{T}_1$ corresponds to the inverse Laplace transform of expression (8a), and $\mathcal{T}_1^{\infty}$ denotes the asymptotic solution given by expression (10). As in previous work (e.g., (*Eskilson*, 1987; *Lamarche and Beauchamp*, 2007b; *Raymond et al.*, 2011a)), we define the asymptotic time t_1 such that E_1 is smaller than 2% for $t > t_1$. The dimensionless asymptotic time is then given by $\tau_1 = t_1 \alpha_1 / R^2$.

To study the impact of the borehole thermal properties on τ_1, consider the case where the temperature is monitored at the borehole wall and the heat source is located at the borehole center. For this configuration, Figure 8 shows τ_1 as a function of the inverses of the relative thermal conductivity κ and diffusivity a. Two general tendencies can be observed for τ_1 depending on the relation between $1/a$ and $1/\kappa$: (i) when $1/a < 1/\kappa$, τ_1 decreases when $1/a$ increases; and (ii) when $1/a > 1/\kappa$, τ_1 increases when $1/a$ increases.

To understand the meaning of these two regimes, consider the borehole and matrix volumetric heat capacities denoted d_1c_1 and d_2c_2, respectively. The relations $1/a < 1/\kappa$ and $1/a > 1/\kappa$ are equivalent to $d_1c_1 > d_2c_2$ and $d_1c_1 < d_2c_2$, respectively, and the transition between the two regimes occurs when $d_1c_1 = d_2c_2$. Consequently, the first regime ($1/a < 1/\kappa$) is characterized by larger values of the volumetric heat capacity in the borehole than in the matrix, which implies that the transient thermal properties of the borehole are dominant factors determining when the standard asymptotic behavior is reached. Increasing $1/a$ until it equals $1/\kappa$ is equivalent to decreasing d_1c_1 until it equals d_2c_2. Consequently, increasing $1/a$ reduces the impact of the borehole transient thermal properties on when asymptotic behavior is reached, and results in a decrease of τ_1. Conversely, in the second regime ($1/a > 1/\kappa$), the transient thermal properties of the matrix are the dominant factors controlling when asymptotic behavior is reached. As an increase of $1/a$ is equivalent to an increase of these matrix properties, it implies that asymptotic behavior is reached later and results in an increase of τ_1.

As standard line-source models consider the heat source to be embedded in the host rock and ignore the presence of the borehole, their corresponding relative thermal conductivity and diffusivity are equal to 1. Considering expression (17) for the standard asymptotic time t_1^{st}, this means that the dimensionless asymptotic time $\tau_1^{st} = 5$. Figure 8 shows that our analysis reproduces well this result in that $\tau_1 = 5$ when $\kappa = 1$ and $a = 1$. Note, however, that we also have $\tau_1 = 5$ for the set of borehole and matrix properties presented in Table 1, which corresponds to a large difference between the true and standard asymptotic times as $t_1 = 23$ hours and $t_1^{st} = 2.9$ hours.

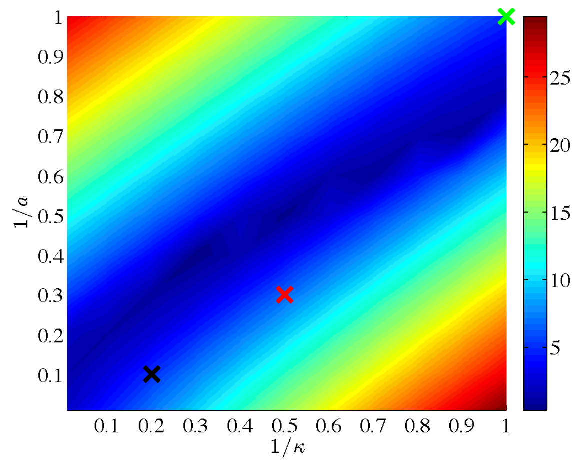

Figure 8: Dimensionless asymptotic time τ_1 as a function of the inverses of the relative thermal conductivity κ and diffusivity a. The black and red crosses represent the values of τ_1 for the sets of parameters presented in Table 1 and Table 2, respectively. The green cross represents the value of τ_1^{st} defined for a homogeneous domain.

For the set of properties in Table 2, we have $\tau_1 = 6.6$ corresponding to $t_1 = 30$ hours, whereas $t_1^{st} = 7.9$ hours. These results show that the borehole thermal properties have a strong impact on the definition of the minimum time required for reaching asymptotic behavior. For the sets of parameters presented in Tables 1 and 2, which have been considered in previous studies, the true asymptotic time is almost 8 and 4 times larger than the asymptotic time evaluated using the standard solution, respectively. Quite importantly, this implies that the duration of borehole thermal experiments must be much longer than the duration usually considered in order to interpret the collected data using asymptotic solutions. If these long-term experiments cannot be conducted, the collected data should be interpreted with exact solutions such as those presented in Section 3.

4.1.2. Impact of the heat source position

We now examine the impact of the position of the line heat source on the dimensionless asymptotic time τ_1. To this end, we consider an experimental configuration where the temperature is again monitored at the borehole wall (as illustrated in Figure 3) assuming the borehole and matrix properties in Table 1. Figure 9 shows the distribution of τ_1 as a function of the heat source position inside the borehole, where a symmetry about the dashed black line is observed. Whereas a radial symmetry would be expected if the temperature sensor were located at the borehole center, its location at the borehole wall results in a different behavior. In particular, we see that (i) τ_1 is minimized when the heat source is at position $(\rho^*_{min}, \theta^*_{min})$, which is the closest location to both the temperature sensor and the borehole-matrix interface; (ii) moving the heat source away from both the temperature sensor and the borehole-matrix interface results in an increase of τ_1, which is observed when the heat source position varies from $(\rho^*_{min}, \theta^*_{min})$ to the borehole center; (iii) moving the heat source further away from the temperature sensor but closer to the borehole-matrix interface implies a smaller increase of τ_1, which is observed when the heat source position varies from the borehole center to $(\rho^*_{max}, \theta^*_{max})$; and (iv) as the distance between the heat source and the borehole-matrix interface decreases, τ_1 decreases as seen when the heat source is moved from the position $(\rho^*_{max}, \theta^*_{max})$ to the left extremity of the dashed black line.

The above observations show that the value of τ_1 depends on the position of the line heat source with respect to the positions of the borehole-matrix interface and the temperature sensor. For dimensionless times larger than τ_1, the monitored temperature can be well described by an asymptotic expres-

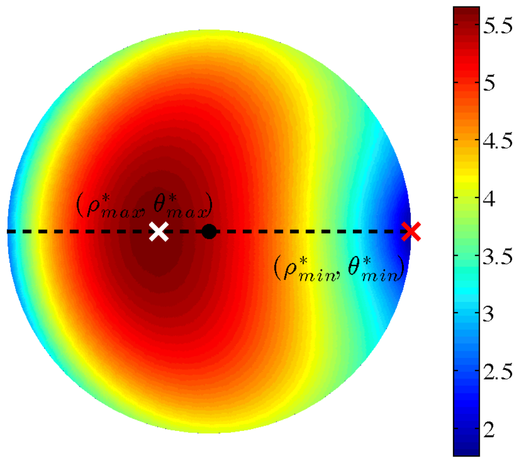

Figure 9: Dimensionless asymptotic time τ_1 plotted as a function of the heat source position inside the borehole, where this position is defined by polar coordinates (ρ^*, θ^*) with $0 \le \rho^* \le 0.9$ and $0° \le \theta^* < 360°$. The minimum and maximum values of τ_1 are observed when the heat source is located at positions $(\rho^*_{min}, \theta^*_{min})$ (red cross) and $(\rho^*_{max}, \theta^*_{max})$ (white cross), respectively. These coordinates are defined as $\rho^*_{min} = 0.9$, $\theta^*_{min} = 0°$, $\rho^*_{max} = 0.22$ and $\theta^*_{max} = 180°$. The black circle indicates the borehole center.

sion that only considers the matrix thermal properties. This implies that τ_1 is minimized in configurations where the matrix thermal properties are dominant. This is the case when the heat source is close to the borehole-matrix interface because heat propagates through both the matrix and the borehole from the very beginning of the experiment. Conversely, when the heat source is located far from the borehole-matrix interface, heat propagates only through the borehole at the beginning of the experiment and the time required to propagate to the matrix results in an increase of τ_1. This is also the case when the heat source is far from the temperature sensor, as heat propagation from the heat source to the sensor is (mostly) done through the borehole. Consequently, increasing the distance between the heat source and the temperature sensor also results in an increase of τ_1.

The results presented in Figure 9 also demonstrate that τ_1 varies between 1.8 and 5.6 for different positions of the heat source in the borehole, which corresponds to a range of variation for t_1 between 8.4 and 26.9 hours. For the case where the heat source is located at the borehole center, $\tau_1 = 5$ and $t_1 = 23$ hours. As a result, in most practical situations, making the assumption that the heat source is located at the borehole center will tend to overestimate the time required to reach asymptotic behavior, which in turn will not pose a danger for corresponding interpretations based on these estimates. In other words, the standard assumption regarding the heat source position will be acceptable for evaluating the temperature at the borehole wall with an asymptotic solution. However, this is only true if the borehole thermal properties are taken into account, which again is not the case with the standard evaluation of the asymptotic time given by equation (17). As seen in Figure 8, assuming identical matrix and borehole thermal properties results in an important underestimation of t_1.

4.2. Error in the estimated matrix thermal conductivity

Asymptotic expressions (11) and (13) for ALS and TRT experiments show that the long-term behavior of the temperature inside a borehole subject to a line heat source can be expressed as

$$\mathcal{T}^{\infty} = m \ln(\tau) + n, \tag{19}$$

where

$$m = \frac{1}{4\pi\kappa}, \tag{20}$$

and, for ALS experiments,

$$n = \frac{1}{4\pi\kappa}\left[\ln(4a) - \gamma\right] - \frac{1}{4\pi}\ln\left(D^2\right) + \frac{\kappa - 1}{4\pi(\kappa+1)}\ln\left[D^2 + \left(1-\rho^{*2}\right)\left(1-\rho^2\right)\right], \tag{21}$$

whereas for TRT experiments,

$$n = \frac{1}{4\pi\kappa}\left[\ln(4a) - \gamma\right] + \frac{1}{4\pi}\left[-\ln\left(D_1\rho_{out}\right) + \frac{\kappa-1}{\kappa+1}\ln\left(D_2\right) + \frac{1}{\kappa_p}\ln\left(\frac{\rho_{out}}{\rho_{in}}\right)\right]. \tag{22}$$

As a result, for times greater than the asymptotic time, the slope of the measured temperature versus $\ln(\tau)$ curve for both experiments can be used to estimate the relative thermal conductivity as follows:

$$\kappa = \frac{1}{4\pi}\left[\frac{\partial \mathcal{T}}{\partial \ln(\tau)}\Big|_{\tau \geq \tau_1}\right]^{-1}. \tag{23}$$

Standard line-source asymptotic solutions based on the assumption that the heat source is at the borehole center and ignoring the borehole thermal properties (e.g., (*Eskilson*, 1987)) yield a similar result, except that in this case we have $n = m\left[\ln(4a) - \gamma\right]$.

We see from the above equations that a major advantage of considering asymptotic solutions is that their slope, and thus the estimation of the matrix thermal conductivity, is not explicitly dependent upon the borehole thermal properties or the position of the heat source in the borehole. However, as observed previously, asymptotic times based on standard solutions may be significantly smaller than those evaluated when the borehole properties are taken into account (Figure 8), meaning that determination of the "correct asymptotic slope" may be significantly in error when these standard asymptotic times are used. To explore this issue, we evaluate the relative error E_2

in the determination of the slope m of the asymptotic solution based on a particular determination of the asymptotic time τ_1, which is quantified by

$$E_2(\tau) = \left| m - \frac{\partial \mathcal{T}_1}{\partial \ln(\tau)}|_{\tau=\tau_1} \right| /m, \tag{24}$$

where $m = 1/(4\pi\kappa)$ is the slope of the asymptotic solution and $\partial \mathcal{T}_1/\partial \ln(\tau)|_{\tau=\tau_1}$ is the slope determined at $\tau = \tau_1$ from the full temperature solution at the borehole wall (equation (8a)), the latter of which we need in order to correctly estimate κ for both ALS and TRT experiments.

We consider the same configuration as before where the temperature is monitored at the borehole wall and the borehole and matrix properties are given by Table 1. For this configuration, Figure 10 shows the distribution of E_2 calculated as a function of the heat source position for two values of the dimensionless asymptotic time τ_1. In Figure 10a, we consider $\tau_1 = \tau_1^{max}$, where τ_1^{max} is the maximum value of τ_1 when the position of the heat source is unknown and when the borehole properties are taken into account. From Figure 9 we see that $\tau_1^{max} = 5.6$, which corresponds to the safest choice of τ_1 when taking into account the borehole thermal properties and the unknown heat source position. Figure 10a shows that E_2 ranges from 5.5% to 13.3% and that the distribution of E_2 as a function of the heat source position is related to the distribution of τ_1 presented in Figure 9. In other words, the time required to obtain a good agreement between the full and asymptotic temperature expressions depends on the heat source position (Figure 9), and a similar dependency is observed for the time required to obtain a good agreement between the slopes of these expressions (Figure 10a). In contrast, Figure 10b shows the results obtained for $\tau_1 = \tau_1^{st}$, where τ_1^{st} is the dimensionless asymptotic time considered from standard line-source models and set to $5/a$. In this case, the overall distribution of E_2 is different from the results presented in Figure 10a with a maximum value equal to 60%.

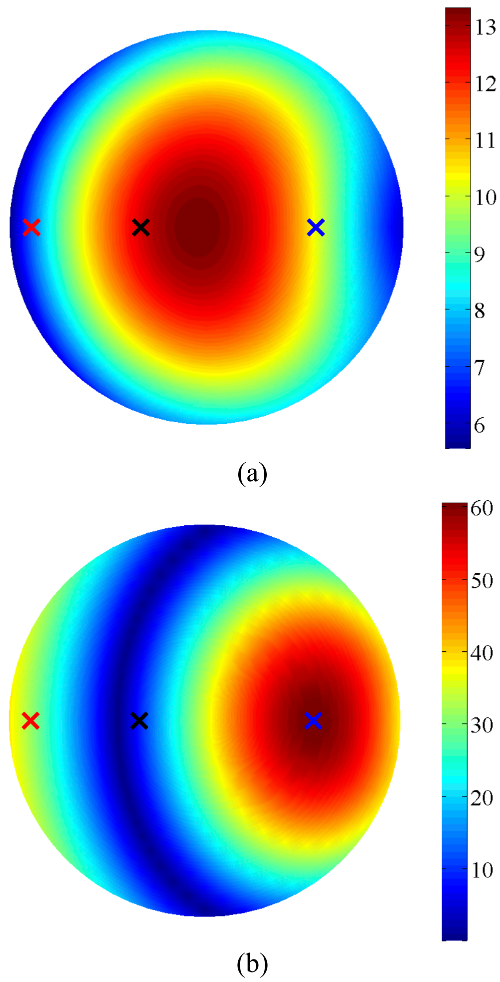

Figure 10: Relative error E_2 defined in expression (24) and plotted as a function of the heat source position inside the borehole, where this position is defined by polar coordinates (ρ^*, θ^*) with $0 \leq \rho^* \leq 0.9$ and $0° \leq \theta^* < 360°$. The dimensionless asymptotic time τ_1 is defined as (a) $\tau_1 = 5.6$ and (b) $\tau_1 = 5/a$. The blue, black and red crosses represent the positions (ρ_1^*, θ_1^*), (ρ_2^*, θ_2^*) and (ρ_3^*, θ_3^*) of the heat source, respectively, defined as $\rho_1^* = 0.5$, $\rho_2^* = 0.3$, $\rho_3^* = 0.8$, $\theta_1^* = 0°$, and $\theta_2^* = \theta_3^* = 180°$.

For a deeper understanding of the results presented in Figure 10, consider the three positions of the heat source represented by the blue, black, and red crosses in Figure 10. The corresponding temperatures and their derivatives are shown in Figure 11 where we see that the asymptotic behavior of the temperature is not reached for $\tau = \tau_1^{st}$, whereas this behavior is reached for $\tau = \tau_1^{max}$ (Figure 11a). This implies a large error in the estimated value of m at $\tau = \tau_1^{st}$ whereas the error is acceptable at $\tau = \tau_1^{max}$ (Figure 11b). Figure 11b also shows that, at $\tau = \tau_1^{st}$, this error is larger when the heat source is located at position (ρ_1^*, θ_1^*) and smaller when the heat source is located at position (ρ_2^*, θ_2^*).

Considering that the temperature inside a borehole can be described by full and asymptotic solutions, the above results show that a good agreement of the slope of these two solutions versus $\ln(\tau)$ can only be obtained for times much larger than traditionally assumed. As the evaluation of the standard asymptotic time is based on line-source models that do not take into account the borehole thermal properties, the value of this time is usually underestimated, as well as the required duration of *in-situ* experiments for obtaining accurate estimates of the thermal conductivity. As shown in the previous section for the set of parameters presented in Table 1, this corresponds to a minimum time around 20 hours, whereas the standard minimum time usually assumed is approximately 3 hours. The results presented in Figure 10 show the importance of a "safe" choice of the asymptotic time as its standard definition can result in an error of 60% in the slope of the temperature expression that is used to obtain *in-situ* matrix thermal conductivity estimate.

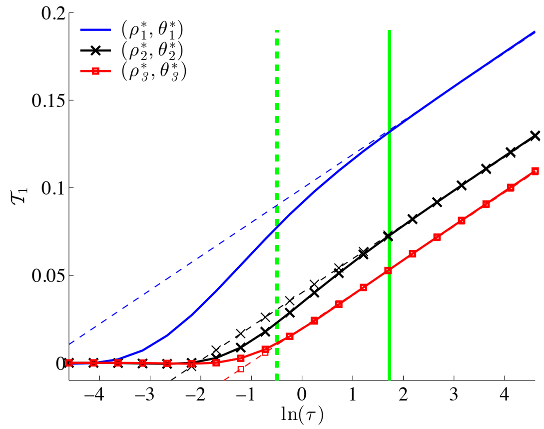

(a)

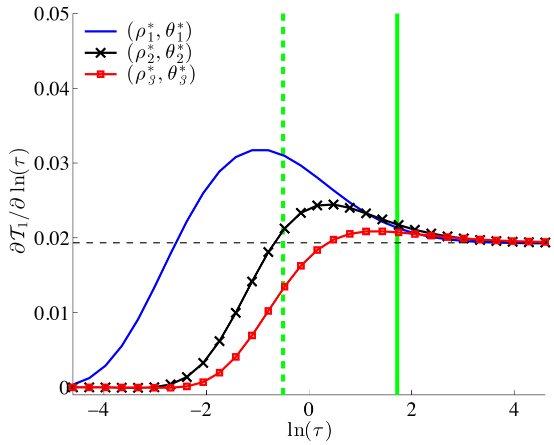

(b)

Figure 11: (a) Dimensionless temperature, and (b) derivative of this temperature with respect to $\ln(\tau)$, plotted as a function of $\ln(\tau)$. The results are obtained with the exact (solid lines) and asymptotic (dashed lines) solutions for three positions of the heat source (ρ^*, θ^*). The vertical dashed and solid green lines represent the standard and maximum dimensionless asymptotic time τ_1^{st} and τ_1^{max}, respectively. Note that, for the asymptotic solution, $\partial\mathcal{T}_1/\partial\ln(\tau)$ is represented by a unique horizontal dashed black line as this expression does not depend on the heat source position (equation (20)).

4.3. Error in the estimated matrix thermal diffusivity

The thermal diffusivity of the matrix is required for studying the transient behavior of heat propagation and its estimation from *in-situ* experiments has been considered in a number of previous studies based on either numerical models or standard line-source models (e.g., *Bozzoli et al.* (2011); *Hu et al.* (2012); *Raymond et al.* (2011); *Sharqawy et al.* (2009); *Wagner and Clauser* (2005); *Zheng et al.* (2013)). Here, for both ALS and TRT experiments, we examine the error in estimates of the relative thermal diffusivity a resulting from incomplete knowledge of the position of the line heat source in the borehole. To this end, we define the relative error E_3 as

$$E_3 = \frac{|a_{true} - a_{est}|}{a_{true}}, \tag{25}$$

where a_{true} is the true relative thermal diffusivity and a_{est} the relative thermal diffusivity estimated assuming some value for the heat source position. We assume that the asymptotic time has been evaluated correctly.

4.3.1. ALS experiments

Expressions (19) through (21) show that the relative thermal diffusivity can be determined from the slope and y-intercept of the asymptotic solution for ALS experiments as follows:

$$a = \frac{1}{4} \exp\left(\beta\right), \tag{26}$$

where

$$\begin{aligned} \beta = {} & \frac{n}{m} + \frac{1}{4\pi m} \ln\left(D^2\right) \\ & - \frac{\kappa - 1}{4\pi m(\kappa + 1)} \ln\left[D^2 + \left(1 - \rho^{*2}\right)\left(1 - \rho^2\right)\right] + \gamma, \end{aligned} \tag{27}$$

and (ρ, θ) and (ρ^*, θ^*) are the temperature sensor and heat source positions, respectively. To examine the errors in the estimated relative diffusivity corresponding to incorrect knowledge of the heat source position, we consider two configurations having borehole and matrix properties presented in Table 1 and with the temperature sensor located at the borehole wall. In the first configuration (Figure 12a), the heat source is assumed to be at the borehole center and the corresponding relative thermal diffusivity is denoted by a_{est}^{ALS1}. This estimate can be deduced from expressions (26) and (27) with $\rho = 1$, $\theta = 0°$, and $\rho^* = 0$, and the result is

$$a_{est}^{ALS1} = \frac{1}{4} \exp\left(\frac{n}{m} + \gamma\right). \tag{28}$$

To evaluate the error in a related to the uncertainty in the heat source position, we use the relative error E_3 defined in expression (25) with a_{true} the true relative thermal diffusivity and a_{est} the relative thermal diffusivity a_{est}^{ALS1}. Figure 12b shows E_3 as a function of the true heat source position which varies over the domain $\Omega_1 = \{(\rho, \theta) : 0 \leq \rho \leq 0.1, 0° \leq \theta < 360°\}$. We see that the error in the relative thermal diffusivity can reach 40% and that the maximum value is obtained when $\rho^* = 0.1$ and $\theta^* = 0°$.

In the second configuration (Figure 12c), the heat source is assumed to be at the maximum distance from the temperature sensor and the corresponding relative thermal diffusivity is denoted by a_{est}^{ALS2}. Again, this estimate can be deduced from expressions (26) and (27) with $\rho = 1$, $\theta = 0°$, $\rho^* = 1$, and $\theta^* = 180°$. This yields

$$a_{est}^{ALS2} = \frac{1}{4} \exp\left[\left(\frac{n}{m}\right) + \gamma\right] 2^{4\kappa/(\kappa+1)}. \tag{29}$$

As before, we use the relative error E_3 with a_{est} defined here as the relative thermal diffusivity a_{est}^{ALS2}. Figure 12d shows this error as a function of the true heat source position which varies over the domain $\Omega_2 = \{(\rho, \theta) : 0.8 \leq \rho \leq 1, 135° \leq \theta \leq 225°\}$. In this case, the relative error in the relative thermal diffusivity estimate can reach a maximum value of 80% for the heat source positions (ρ_1^*, θ_1^*) and (ρ_2^*, θ_2^*) with $\rho_1^* = 0.8$, $\theta_1^* = 135°$, $\rho_2^* = 0.8$, and $\theta_2^* = 225°$. Note that this maximum error is related to a larger area than before as the domain Ω_2 is characterized by a larger area than the domain Ω_1. When Ω_2 is reduced to a domain with the same area as Ω_1, the range of variation of E_3 is similar for the two configurations and its maximal value is around 40%.

The results presented in Figure 12 show that the relative thermal diffusivity estimated with ALS experiments is sensitive to small variations of the line heat source position. This implies that an accurate *in-situ* evaluation of the thermal diffusivity requires reducing the uncertainty on the position of the heating cable used in these experiments. When this cable is assumed to be at the borehole center, the uncertainty in its position may be reduced by using some form of centralizer (e.g., *Read et al.* (2014)). On the other hand, when the heat source is assumed to be at the maximum distance from the temperature sensor, the heating cable might be located between the borehole wall and a liner used to seal the borehole. The latter corresponds to the extension of a recently conducted experiment where co-located heater and temperature measurements have been achieved with recent DTS technologies (e.g., *Coleman et al.* (2015)). Although *in-situ* experiments should be conducted in future work to confirm this conclusion, the second studied configuration seems to be the most adapted to reduce the uncertainty on

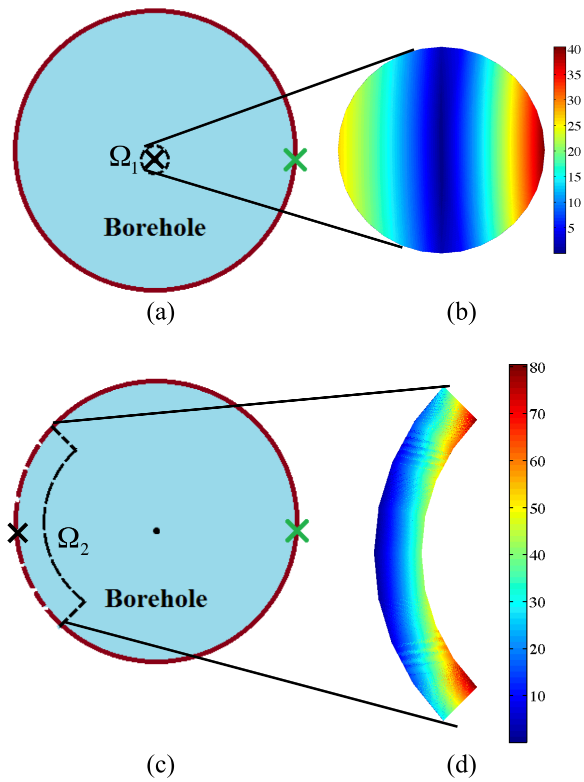

Figure 12: (a) and (c) Studied borehole configurations for ALS experiments. The small black circle represents the borehole center, the green cross the temperature sensor, and the black cross the assumed heat source position. (b) and (d) The corresponding relative error E_3 in the relative thermal diffusivity plotted as a function of the true heat source position which varies about its assumed position over the domains Ω_1 and Ω_2, respectively.

the heat source position and its impact on the subsurface thermal diffusivity estimated from borehole thermal experiments using ALS method.

4.3.2. TRT experiments

We now evaluate the errors in the estimated relative thermal diffusivity from incorrect knowledge of the heat source position for TRT experiments. To this end, we consider a configuration with the borehole-matrix and U-pipe properties presented in Tables 2 and 3, respectively, and we assume that the U-pipe is centered in the borehole. Expressions (19), (20), and (22) demonstrate that the relative thermal diffusivity can be determined from the slope and y-intercept of the asymptotic solution for TRT experiments as follows:

$$
\begin{aligned}
a_{est}^{TRT} &= \frac{1}{4} \exp\left(\frac{n}{m} + \gamma\right) \\
&\times \exp\left\{\kappa \left[\ln\left(D_1 \rho_{out}\right) - \frac{\kappa - 1}{\kappa + 1} \ln\left(D_2\right) - \frac{1}{\kappa_p} \ln\left(\frac{\rho_{out}}{\rho_{in}}\right)\right]\right\}.
\end{aligned} \tag{30}
$$

As with ALS experiments, we use the error E_3 defined in equation (25) to evaluate the error on the relative thermal diffusivity when the assumption concerning the heat source position is incorrect. Here, a_{true} is the true value of a and a_{est} is the value estimated from expression (30) assuming that the U-pipe is centered in the borehole. We consider a first experiment corresponding to the configuration in Figure 6a with a variation of the dimensionless distance ρ_c between the borehole center and the U-pipe center. In this case, the value of ρ_c ranges from 0 to 0.56, where the maximum value corresponds to a configuration with the pipes in contact with the borehole-matrix interface. Figure 13a shows that increasing ρ_c implies an increase in the error because the U-pipe is further from its assumed position. This figure also shows that E_3 reaches the maximum value of 38% when ρ_c reaches its maximal value 0.56. In a second configuration, we consider several values of both ρ_c and θ_0, which correspond to moving the U-pipe away from the borehole center and rotating the U-pipe around its center, respectively. In this case, and considering a full rotation of the U-pipe, the maximum value of ρ_c is 0.26, which corresponds to having pipe 2 in contact with the borehole-matrix interface when $\theta_0 = 90°$. As before, Figure 13b shows that E_3 increases when ρ_c increases. This figure also shows that the U-pipe angle impacts the relative error in a, which ranges, for example, from 8% to 18.6% for $\rho_c = 0.26$.

For ALS experiments (Section 4.3.1), we saw that a small variation of the heat source position from its assumed position can result in an error of 40% in the relative thermal diffusivity. This means that large errors are expected for larger differences between the true and assumed heat source positions. Improving the accuracy of the thermal diffusivity estimated with these experiments requires a better control of the heating cable position. Conversely, for TRT experiments, 40% corresponds to the maximum error obtained when considering all of the possible positions of the U-pipe in the borehole. For the set of parameters considered in this study, these results show that TRT experiments are more suitable than ALS experiments for estimating the subsurface thermal diffusivity, which is largely due to the small degree of variability of the U-pipe position in TRT experiments in comparison with the heating cable position in ALS experiments. However, larger errors could be expected if a U-pipe having a small size in comparison with the borehole radius were considered, thus leading to greater uncertainty regarding its true position in the borehole.

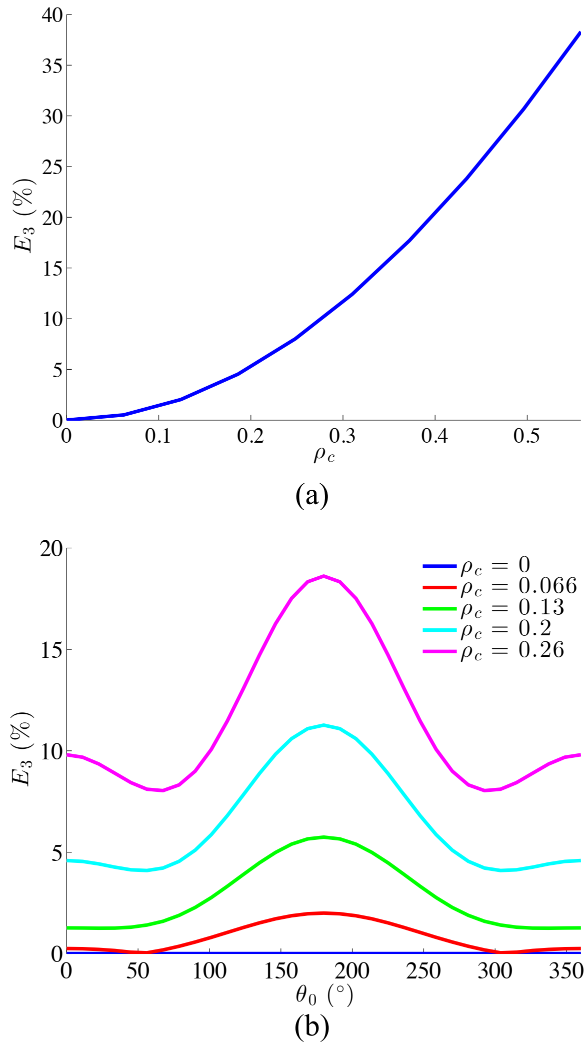

Figure 13: Relative error E_3 in the estimated relative thermal diffusivity for TRT experiments assuming that the U-pipe is centered in the borehole. This is plotted as a function of the true position of the U-pipe with (a) $0 \leq \rho_c \leq 0.56$, $\theta_c = 90°$, and $\theta_0 = 0°$, and (b) $0 \leq \rho_c \leq 0.26$, $\theta_c = 90°$, and $0° \leq \theta_0 < 360°$.

5. Discussion and conclusions

We have developed in this paper new Laplace- and time-domain analytical expressions for interpreting borehole thermal experiments. Using these expressions, we showed that the typical practice of ignoring the borehole thermal properties, through the consideration of simplified asymptotic solutions, can result in a significant underestimation of the time required to reach asymptotic behavior. Quite importantly, this means that the borehole experiments should be conducted for times much larger than traditionally assumed when using such simplified solutions, or that they should be interpreted with exact solutions like the Laplace-domain ones developed in this work. We also showed that the uncertainty related to the position of the heat source in the borehole does not significantly impact the value of the asymptotic time when the borehole thermal properties are properly taken into account. However, the combined effects of ignoring the borehole properties and not knowing the heat source position result in an error of up to 60% in the estimate of the slope of the measured temperature curve, which is used to evaluate the subsurface thermal conductivity. Using asymptotic time values that take into account the borehole thermal properties and heat-source-position uncertainty enables us to reduce this error to only 10%. Concerning the subsurface thermal diffusivity, we saw a significant impact of the heat source position on the estimation of this parameter from ALS experiments, in that sense that errors of 40% were obtained in our simulations. Conversely, 40% corresponds to the maximum error in the relative thermal diffusivity estimated with TRT experiments for any position of the U-pipe.

The results presented in this work considered the interpretation of the heating period during borehole thermal experiments. Based on the relatively rapid homogenization of the borehole temperature after heating has stopped (*Raymond et al.*, 2011b), some researchers have suggested that the cooling period may be better adapted for analyzing temperature measurements for the estimation of subsurface thermal properties (e.g., (*Raymond et al.*, 2011b; *Pehme et al.*, 2013)). The corresponding justification is that, during cooling, errors related to movement of the temperature sensor over the course of measurements will be reduced because the variation of temperature inside the borehole is smaller than during the heating period. As we considered a fixed position of the temperature sensor in our study, these aspects were not considered. That is, when studying the effects of the heat source position, we evaluated the impact of a wrongly assumed position that was fixed during the entire experiment. However, analyzing the consequences of displacement of the sensor should be conducted as future work.

As additional extensions of this research, we plan to develop solutions that account for the presence of advective flow in the formation, which is important for interpreting borehole thermal experiments in fractured rocks where hydraulically-active fractures intersect the borehole. We also plan to focus further on the interpretation of data collected during both ALS and TRT experiments, in the context of using the proposed solutions to develop a systematic strategy to invert for subsurface thermal properties. Finally, a long-term goal of our work is to investigate how analytical solutions may be developed for cross-borehole thermal experiments in fractured rock in order to evaluate characteristics of the fracture network. Here, existing models for hydraulic experiments between boreholes (e.g., (*Roubinet et al.*, 2015)) and heat transport in fracture-matrix systems (e.g., (*Ruiz Martinez et al.*, 2014)) could be employed.

Acknowledgments

We thank the Fondation Herbette for supporting a visit of B. Parker to the University of Lausanne.

Appendix A. Green's functions

Appendix A.1. Borehole domain

We wish to derive the Green's function $\mathcal{T}_1^*(\rho,\rho',\theta,\theta',\tau,\tau')$ associated with equation (5a), and subject to the initial conditions

$$\mathcal{T}_1^*(\tau=0)=0, \quad \mathcal{T}_1^*(\tau=\tau')=0, \tag{A.1a}$$

and the boundary conditions

$$\mathcal{T}_1^*(\rho\to 0)<\infty, \quad \frac{\partial \mathcal{T}_1^*}{\partial \rho}(\rho=1)=0. \tag{A.1b}$$

Defining the Laplace transform of a function $f(t)$ as

$$\bar{f}(s)=\int_0^\infty f(t)e^{-st}\mathrm{d}t, \tag{A.2}$$

the Laplace transform of $\mathcal{T}_1^*$ satisfies

$$\begin{aligned} s\bar{\mathcal{T}}_1^* - \frac{\partial^2\bar{\mathcal{T}}_1^*}{\partial\rho^2} - \frac{1}{\rho}\frac{\partial\bar{\mathcal{T}}_1^*}{\partial\rho} - \frac{1}{\rho^2}\frac{\partial^2\bar{\mathcal{T}}_1^*}{\partial\theta^2} \\ = \delta(\rho-\rho',\theta-\theta')e^{-s\tau'}/\rho, \end{aligned} \tag{A.3}$$

and is subject to the boundary conditions

$$\bar{\mathcal{T}}_1^*(\rho\to 0)<\infty, \quad \frac{\partial \bar{\mathcal{T}}_1^*}{\partial \rho}(\rho=1)=0. \tag{A.4}$$

Based on the derivation method used in *Regenstreif* (1977) for steady-state equation, we assume that $\bar{\mathcal{T}}_1^*$ can be expressed as

$$\bar{\mathcal{T}}_1^* = \sum_{m=0}^{\infty} f_m(\rho, \rho', s, \tau') \cos[m(\theta - \theta')]. \tag{A.5}$$

This expression is introduced in equation (A.3) which is then multiplied by $\cos[n(\theta - \theta')]$ and integrated over θ from 0 to 2π. This leads to, for $m = 0$,

$$s f_0^i - \frac{\partial^2 f_0^i}{\partial \rho^2} - \frac{1}{\rho}\frac{\partial f_0^i}{\partial \rho} = \frac{\delta(\rho - \rho')}{2\pi\rho} e^{-s\tau'} \tag{A.6a}$$

and, for $m \geq 1$,

$$\left(s + \frac{1}{\rho^2} m^2\right) f_m^i - \frac{\partial^2 f_m^i}{\partial \rho^2} - \frac{1}{\rho}\frac{\partial f_m^i}{\partial \rho} = \frac{\delta(\rho - \rho')}{\pi\rho} e^{-s\tau'}, \tag{A.6b}$$

where the latter equations are subject to the boundary conditions

$$f_0^1(\rho \to 0) < \infty, \quad \frac{\partial f_0^1}{\partial \rho}(\rho = 1) = 0, \tag{A.7a}$$

and

$$f_m^1(\rho \to 0) < \infty, \quad \frac{\partial f_m^1}{\partial \rho}(\rho = 1) = 0, \quad m \geq 1. \tag{A.7b}$$

For $\rho \neq \rho'$, considering equations (A.6) associated with boundary conditions (A.7), we obtain the following expressions for f_0^1 and f_m^1:

$$f_0^1 = \begin{cases} A_0 I_0(q_1\rho), & \rho < \rho', \\ D_0 \left[K_0(q_1\rho) + G_0(q_1) I_0(q_1\rho)\right], & \rho > \rho', \end{cases} \tag{A.8a}$$

and

$$f_m^1 = \begin{cases} A_m I_m(q_1\rho), & \rho < \rho', \\ D_m \left[K_m(q_1\rho) + G_m(q_1) I_m(q_1\rho)\right], & \rho > \rho', \end{cases} \tag{A.8b}$$

with $q_1 = \sqrt{s}$. Here the functions $I_m(.)$ and $K_m(.)$ are the modified Bessel functions of the first and second kind, respectively, and the function $G_m(q_i)$ ($i = 1, 2$) is defined as $G_m(q_i) = G^1_m(q_i)/G^2_m(q_i)$ with the functions $G^1_m(q_i)$ and $G^2_m(q_i)$ expressed as

$$G^1_m(q_i) = K_{m+1}(q_i) - mK_m(q_i)/q_i, \tag{A.9a}$$

and

$$G^2_m(q_i) = I_{m+1}(q_i) + mI_m(q_i)/q_i. \tag{A.9b}$$

Finally, continuity conditions for $\rho = \rho'$ are enforced and the final expressions for f^1_0 and f^1_m are

$$f^1_0 = \begin{cases} \frac{e^{-s\tau'}}{2\pi} I_0(q_1\rho)F^1_0(\rho'), & \rho < \rho', \\ \frac{e^{-s\tau'}}{2\pi} I_0(q_1\rho')F^1_0(\rho), & \rho > \rho', \end{cases} \tag{A.10a}$$

and

$$f^1_m = \begin{cases} \frac{e^{-s\tau'}}{\pi} I_m(q_1\rho)F^1_m(\rho'), & \rho < \rho', \\ \frac{e^{-s\tau'}}{\pi} I_m(q_1\rho')F^1_m(\rho), & \rho > \rho', \end{cases} \tag{A.10b}$$

where the function $F^1_m(\rho)$ is defined as $F^1_m = K_m(q_1\rho) + G_m(q_1)I_m(q_1\rho)$. By using these expressions in (A.5), we obtain the following final expression for $\bar{\mathcal{T}}^*_1$:

$$\bar{\mathcal{T}}^*_1 = \frac{e^{-s\tau'}}{2\pi} I_0(q_1\rho)F^1_0(\rho') \tag{A.11a}$$
$$+ \frac{e^{-s\tau'}}{\pi} \sum_{m=1}^{\infty} I_m(q_1\rho)F^1_m(\rho') \cos\left[m(\theta - \theta')\right], \quad \rho < \rho',$$

and

$$\bar{\mathcal{T}}^*_1 = \frac{e^{-s\tau'}}{2\pi} I_0(q_1\rho')F^1_0(\rho) \tag{A.11b}$$
$$+ \frac{e^{-s\tau'}}{\pi} \sum_{m=1}^{\infty} I_m(q_1\rho')F^1_m(\rho) \cos\left[m(\theta - \theta')\right], \quad \rho > \rho'.$$

Appendix A.2. Matrix domain

We consider now the Green's function $\mathcal{T}_2^*(\rho, \rho', \theta, \theta', \tau, \tau')$ associated with equation (5b), and subject to the initial conditions

$$\mathcal{T}_2^*(\tau = 0) = 0, \quad \mathcal{T}_2^*(\tau = \tau') = 0, \tag{A.12a}$$

and the boundary conditions

$$\frac{\partial \mathcal{T}_2^*}{\partial \rho}(\rho = 1) = 0, \quad \mathcal{T}_2^*(\rho \to \infty, \theta, \tau) = 0. \tag{A.12b}$$

The Laplace transform of $\mathcal{T}_2^*$ satisfies

$$\begin{aligned} & s\bar{\mathcal{T}}_2^* - a\frac{\partial^2 \bar{\mathcal{T}}_2^*}{\partial \rho^2} - \frac{a}{\rho}\frac{\partial \bar{\mathcal{T}}_2^*}{\partial \rho} - \frac{a}{\rho^2}\frac{\partial^2 \bar{\mathcal{T}}_2^*}{\partial \theta^2} \\ & = \frac{\delta(\rho - \rho', \theta - \theta')}{\rho} e^{-s\tau'} \end{aligned} \tag{A.13}$$

and is subject to the boundary conditions

$$\frac{\partial \bar{\mathcal{T}}_2^*}{\partial \rho}(\rho = 1) = 0, \quad \bar{\mathcal{T}}_2^*(\rho \to \infty) = 0. \tag{A.14}$$

Applying the same methodology as in Appendix A.1, $\bar{\mathcal{T}}_2^*$ is expressed as

$$\begin{aligned} \bar{\mathcal{T}}_2^* = & \frac{e^{-s\tau'}}{2\pi a} K_0(q_2\rho') F_0^2(\rho) \\ & + \frac{e^{-s\tau'}}{\pi a} \sum_{m=1}^{\infty} K_m(q_2\rho') F_m^2(\rho) \cos[m(\theta - \theta')], \quad \rho < \rho', \end{aligned} \tag{A.15a}$$

and

$$\begin{aligned} \bar{\mathcal{T}}_2^* = & \frac{e^{-s\tau'}}{2\pi a} K_0(q_2\rho) F_0^2(\rho') \\ & + \frac{e^{-s\tau'}}{\pi a} \sum_{m=1}^{\infty} K_m(q_2\rho) F_m^2(\rho') \cos[m(\theta - \theta')], \quad \rho > \rho', \end{aligned} \tag{A.15b}$$

with q_2 and $F_m^2(\rho)$ defined as $q_2 = \sqrt{s/a}$ and $F_m^2(\rho) = I_m(q_2\rho) + K_m(q_2\rho)/G_m(q_2)$.

Appendix B. General Laplace-domain temperature expressions

Appendix B.1. Temperature integral expressions

It is possible to derive an analytical expression for the dimensionless temperature $\mathcal{T}_1$ by (i) rewriting equation (5a) in terms of the variables ρ', θ' and τ' with a source term at position (ρ^*, θ^*) at time τ^*; (ii) multiplying this equation by the elementary solution $\mathcal{T}_1^*$ defined in Appendix A.1; and (iii) integrating over the domain $\tilde{\Omega}_b$ and until time τ. Integrating by parts each term, and using the initial and boundary conditions related to $\mathcal{T}_1$ and $\mathcal{T}_1^*$ and the second continuity condition (6c), $\mathcal{T}_1$ is expressed as

$$\mathcal{T}_1(\rho, \theta, \tau) = \int_0^\tau u(\tau^* - \tau') \mathcal{T}^*_{1\,|\rho'=\rho^*, \theta'=\theta^*} \mathrm{d}\tau' + \int_0^\tau \int_0^{2\pi} g(\theta', \tau') \mathcal{T}^*_{1\,|\rho'=1} \mathrm{d}\theta' \mathrm{d}\tau'. \tag{B.1a}$$

Applying the same methodology for the dimensionless temperature $\mathcal{T}_2$ with its related Green's function $\mathcal{T}_2^*$, their related initial and boundary conditions, and the second continuity condition (6c), we obtain the following expression:

$$\mathcal{T}_2(\rho, \theta, \tau) = -\frac{a}{\kappa} \int_0^\tau \int_0^{2\pi} g(\theta', \tau') \mathcal{T}^*_{2\,|\rho'=1} \mathrm{d}\theta' \mathrm{d}\tau'. \tag{B.1b}$$

Appendix B.2. Temperature final expressions

From expressions (B.1), the Laplace transform of $\mathcal{T}_1$ and $\mathcal{T}_2$ are expressed as

$$\bar{\mathcal{T}}_1(\rho, \theta, s) = \frac{1 - e^{-s\tau^*}}{s} \bar{\mathcal{T}}^*_{1\,|\rho'=\rho^*, \theta'=\theta^*, \tau'=0} + \int_0^{2\pi} \bar{\mathcal{T}}^*_{1\,|\rho'=1, \tau'=0} \bar{g}(\theta', \tau) \mathrm{d}\theta' \tag{B.2a}$$

and

$$\bar{\mathcal{T}}_2(\rho,\theta,s) = -\frac{a}{\kappa}\int_0^{2\pi} \bar{\mathcal{T}}^*_{2\,|\rho'=1,\tau'=0}\bar{g}(\theta',\tau)\mathrm{d}\theta', \tag{B.2b}$$

and the first continuity condition (6c) can be expressed as

$$\begin{aligned}&\frac{1-e^{-s\tau^*}}{s}\bar{\mathcal{T}}^*_{1\,|\rho=1,\rho'=\rho^*,\theta'=\theta^*,\tau'=0}\\ &+\int_0^{2\pi}\bar{\mathcal{T}}^*_{1\,\rho=1,\rho'=1,\tau'=0}\bar{g}(\theta',\tau)\mathrm{d}\theta'\\ &=-\frac{a}{\kappa}\int_0^{2\pi}\bar{\mathcal{T}}^*_{2\,\rho=1,\rho'=1,\tau'=0}\bar{g}(\theta',\tau)\mathrm{d}\theta'.\end{aligned} \tag{B.3}$$

When substituting $\bar{\mathcal{T}}^*_1$ and $\bar{\mathcal{T}}^*_2$ in (B.3) with their expressions (A.11) and (A.15), (B.3) is rewritten as

$$\begin{aligned}&\left[\frac{I_0(q_1)}{I_1(q_1)}+\frac{K_0(q_2)}{\sigma K_1(q_2)}\right]\int_0^{2\pi}\bar{g}\mathrm{d}\theta'\\ &+2\sum_{m=1}^{\infty}\left[\frac{I_m(q_1)}{G^2_m(q_1)}+\frac{K_m(q_2)}{\sigma G^1_m(q_2)}\right]\int_0^{2\pi}\cos\left[m(\theta-\theta')\right]\bar{g}\mathrm{d}\theta'\\ =&-\frac{1-e^{-s\tau^*}}{s}\frac{I_0(q_1\rho^*)}{I_1(q_1)}\\ &-\frac{2\left(1-e^{-s\tau^*}\right)}{s}\sum_{m=1}^{\infty}\frac{I_m(q_1\rho^*)}{G^2_m(q_1)}\cos[m(\theta-\theta^*)],\end{aligned} \tag{B.4}$$

where σ is defined as $\sigma=\kappa/\sqrt{a}$, and the functions $G^1_m(q_1)$ and $G^2_m(q_2)$ are defined in (A.9).

(B.4) is then integrated over θ, yielding

$$\int_0^{2\pi}\bar{g}\mathrm{d}\theta' = -\frac{1-e^{-s\tau^*}}{s}\frac{\sigma K_1(q_2)I_0(q_1\rho^*)}{\sigma K_1(q_2)I_0(q_1)+K_0(q_2)I_1(q_1)} \tag{B.5a}$$

and

$$\begin{aligned}\int_0^{2\pi}\cos(m(\theta-\theta'))\bar{g}\mathrm{d}\theta' &= -\frac{1-e^{-s\tau^*}}{s}\\ &\times\frac{\sigma I_m(q_1\rho^*)G^1_m(q_2)\cos[m(\theta-\theta^*)]}{\sigma I_m(q_1)G^1_m(q_2)+K_m(q_2)G^2_m(q_1)}.\end{aligned} \tag{B.5b}$$

Finally, expressions (B.5) can be used to obtain the following final expressions for $\bar{\mathcal{T}}_1$ and $\bar{\mathcal{T}}_2$:

$$\bar{\mathcal{T}}_1 = \frac{1-e^{-s\tau^*}}{2\pi s} I_0(q_1\rho) H_0(\rho^*) + \frac{1-e^{-s\tau^*}}{\pi s} \sum_{m=1}^{\infty} I_m(q_1\rho) H_m(\rho^*) \cos\left[m(\theta-\theta^*)\right], \quad \rho < \rho^*, \tag{B.6a}$$

$$\bar{\mathcal{T}}_1 = \frac{1-e^{-s\tau^*}}{2\pi s} I_0(q_1\rho^*) H_0(\rho) + \frac{1-e^{-s\tau^*}}{\pi s} \sum_{m=1}^{\infty} I_m(q_1\rho^*) H_m(\rho) \cos\left[m(\theta-\theta^*)\right], \quad \rho > \rho^*, \tag{B.6b}$$

and

$$\bar{\mathcal{T}}_2 = \frac{1-e^{-s\tau^*}}{2\pi s} I_0(q_1\rho^*) \frac{K_0(q_2\rho)}{K_0(q_2)} h_0 + \frac{1-e^{-s\tau^*}}{\pi s} \sum_{m=1}^{\infty} I_m(q_1\rho^*) \frac{K_m(q_2\rho)}{K_m(q_2)} h_m \cos\left[m(\theta-\theta^*)\right]. \tag{B.6c}$$

In expressions (B.6), the function $H_m(\rho)$ is defined as

$$H_m(\rho) = K_m(q_1\rho) + \beta_m I_m(q_1\rho) \tag{B.7}$$

with

$$\beta_m = \frac{-\sigma K_m(q_1) G_m^1(q_2) + K_m(q_2) G_m^1(q_1)}{K_m(q_2) G_m^2(q_1) + \sigma I_m(q_1) G_m^1(q_2)}, \tag{B.8}$$

and h_m is a particular value of the function $H_m(\rho)$ defined as $h_m = H_m(1)$.

Appendix C. Temperature expressions for borehole thermal experiments

Appendix C.1. Asymptotic expression for ALS experiments

In this section, we wish to derive $\mathcal{T}_1^{\infty}$, the time-domain analytical expression that describes the asymptotic behavior of the temperature monitored during ALS experiments. For deriving this expression, we use the exact Laplace-domain solution (8a) corresponding to a heat source from $\tau = 0$ to τ^*. This solution can be rewritten as

$$\bar{\mathcal{T}}_1(\rho, \theta, s) = \left(1 - e^{-s\tau^*}\right) \bar{\mathcal{T}}_1^h(\rho, \theta, s), \tag{C.1}$$

with $\bar{\mathcal{T}}_1^h$ the Laplace-domain solution corresponding to a heat source from $\tau = 0$ to ∞ and defined as

$$\bar{\mathcal{T}}_1^h(\rho, \theta, s) = \begin{cases} \omega_1 / \left(2\pi s\right) + S_1 / \left(\pi s\right), & \rho < \rho^*, \\ \omega_2 / \left(2\pi s\right) + S_2 / \left(\pi s\right), & \rho > \rho^*. \end{cases} \tag{C.2}$$

From expression (C.1), $\mathcal{T}_1^\infty$ can be expressed as

$$\begin{aligned} \mathcal{T}_1^\infty(\rho, \theta, \tau) = & \mathcal{T}_1^{h,\infty}(\rho, \theta, \tau) \\ & - u\left(\tau - \tau^*\right) \mathcal{T}_1^{h,\infty}(\rho, \theta, \tau - \tau^*), \end{aligned} \tag{C.3}$$

where $\mathcal{T}_1^{h,\infty}$ describes the asymptotic behavior of $\mathcal{T}_1^h$, which is the inverse Laplace transform of $\bar{\mathcal{T}}_1^h$.

For deriving an analytical expression of $\mathcal{T}_1^\infty$, we need to derive an analytical expression of $\mathcal{T}_1^{h,\infty}$. To this end, we consider the following approximations of the Bessel functions $I_m(x)$ and $K_m(x)$ for small values of x (*Abramowitz and Stegun*, 1972):

$$I_m(x) \sim \frac{1}{m!} \left(\frac{x}{2}\right)^m \tag{C.4a}$$

and

$$K_m(x) \sim \frac{(m-1)!}{2} \left(\frac{x}{2}\right)^{-m}. \tag{C.4b}$$

Using these approximations for small values of the Laplace variable s, the Laplace transform of the asymptotic solution $\mathcal{T}_1^{h,\infty}$ is expressed as

$$\begin{aligned}\bar{\mathcal{T}}_1^{h,\infty}(\rho,\theta,s) =& \frac{1}{2\pi s}\left[K_0(q_1\rho^*) - K_0(q_1) + K_0(q_2)/\kappa\right] \\ &+ \frac{1}{2\pi s}\sum_{m=1}^{\infty} s_m^1 \cos\left[m(\theta-\theta^*)\right], \quad \rho < \rho^*,\end{aligned} \tag{C.5a}$$

and

$$\begin{aligned}\bar{\mathcal{T}}_1^{h,\infty}(\rho,\theta,s) =& \frac{1}{2\pi s}\left[K_0(q_1\rho) - K_0(q_1) + K_0(q_2)/\kappa\right] \\ &+ \frac{1}{2\pi s}\sum_{m=1}^{\infty} s_m^2 \cos\left[m(\theta-\theta^*)\right], \quad \rho > \rho^*,\end{aligned} \tag{C.5b}$$

where the terms s_m^1 and s_m^2 are defined as

$$s_m^1 = \frac{1}{m}\left[\left(\frac{\rho}{\rho^*}\right)^m - \frac{\kappa-1}{\kappa+1}(\rho\rho^*)^m\right] \tag{C.6a}$$

and

$$s_m^2 = \frac{1}{m}\left[\left(\frac{\rho^*}{\rho}\right)^m - \frac{\kappa-1}{\kappa+1}(\rho\rho^*)^m\right]. \tag{C.6b}$$

From (C.5), $\mathcal{T}_1^{h,\infty}$ can be derived analytically as follows:

$$\begin{aligned}\mathcal{T}_1^{h,\infty}(\rho,\theta,\tau) =& \frac{1}{4\pi}\left[\Gamma\left(0,\frac{\rho^{*2}}{4\tau}\right) - \Gamma\left(0,\frac{1}{4\tau}\right) + \frac{1}{\kappa}\Gamma\left(0,\frac{1}{4a\tau}\right)\right] \\ &+ \frac{1}{2\pi}\sum_{m=1}^{\infty} s_m^1 \cos\left[m(\theta-\theta^*)\right], \quad \rho < \rho^*\end{aligned} \tag{C.7a}$$

and

$$\begin{aligned}\mathcal{T}_1^{h,\infty}(\rho,\theta,\tau) =& \frac{1}{4\pi}\left[\Gamma\left(0,\frac{\rho^{2}}{4\tau}\right) - \Gamma\left(0,\frac{1}{4\tau}\right) + \frac{1}{\kappa}\Gamma\left(0,\frac{1}{4a\tau}\right)\right] \\ &+ \frac{1}{2\pi}\sum_{m=1}^{\infty} s_m^2 \cos\left[m(\theta-\theta^*)\right], \quad \rho > \rho^*.\end{aligned} \tag{C.7b}$$

As our solution is developed for large times, we consider that the gamma function $\Gamma(0,x)$ can be approximated as $\Gamma(0,x) = -\ln(x) - \gamma$ (*Abramowitz and Stegun*, 1972). Considering, in addition, the following relationship

$$\sum_{m=1}^{\infty} \frac{a^m \cos(m\phi)}{m} = -\frac{1}{2} \ln\left[1 - 2a\cos(\phi) + a^2\right], \tag{C.8}$$

expression (C.7) is rewritten as

$$\begin{aligned} \mathcal{T}_1^{h,\infty}(\rho,\theta,\tau) = & \frac{1}{4\pi\kappa}\left[\ln(\tau) + \ln(4a) - \gamma - \kappa\ln\left(D^2\right)\right] \\ & + \frac{\kappa-1}{4\pi(\kappa+1)} \ln\left[D^2 + \left(1-\rho^{*2}\right)\left(1-\rho^2\right)\right], \end{aligned} \tag{C.9}$$

where D, the distance between the sensor and heat source, is expressed as $D = \sqrt{\rho^{*2} - 2\rho\rho^*\cos(\theta-\theta^*) + \rho^2}$.

Using expression (C.9) in (C.3) enables us to obtain an analytical expression of the time-domain asymptotic solution $\mathcal{T}_1^{\infty}$.

Appendix C.2. Temperature expressions for TRT methods

Typically, the temperature T_{TRT} monitored during TRT experiments is defined as the average of the water temperature T_f^i $(i = 1, 2)$ monitored at the two extremities of the U-pipe. For each pipe i, this temperature is usually expressed through a pipe resistance model as a function of T_p^i, the temperature averaged over the external surface of pipe i (Figure 5c). This yields

$$T_f^i = T_p^i + Q_i R_p, \tag{C.10}$$

where Q_i is the heat flux from the fluid to the external surface of pipe i, and R_p is the pipe thermal resistance that can be defined as $R_p = [\ln(r_{out}/r_{in})]/(2\pi K_p)$ (e.g., (*Lamarche et al.*, 2010)).

Using the temperature expression developed in Section 2, we wish to derive a new analytical expression for T_p^i. As the heat equations (5) are linear, the presence of several source terms can be considered by superposing the solution for each source term as follows:

$$T_p^i = \sum_{j=1}^{N} T_p^{i,j}, \tag{C.11}$$

with N the number of source terms (here, $N = 2$), and $T_p^{i,j}$ the mean temperature on the external surface of pipe i subject to a heat source at pipe j. Considering the dimensionless temperature $\mathcal{T}_p^{i,j} = K_1 T_p^{i,j}/Q_j$ and the average temperature $\mathcal{T}_p^{av,j} = \left(\mathcal{T}_p^{1,j} + \mathcal{T}_p^{2,j}\right)/2$, the temperature measured during TRTs can be expressed as

$$\begin{aligned} T_{TRT} = &(Q_1 \mathcal{T}_p^{av,1} + Q_2 \mathcal{T}_p^{av,2})/K_1 \\ &+ (Q_1 + Q_2) R_p/2, \end{aligned} \tag{C.12}$$

and its dimensionless formulation is defined as $\mathcal{T}_{TRT} = T_{TRT} K_1/Q$ with $Q = Q_1 + Q_2$.

As $\mathcal{T}_p^{i,j}$ is the dimensionless temperature averaged over the external surface of pipe i subject to a heat source at pipe j, it can be expressed as $\mathcal{T}_p^{i,j} = \frac{1}{L}\int_L \mathcal{T}_{1,j} \mathrm{d}l_i$ where L is the circumference of the outer external surface, $\mathrm{d}l_i$ the integral variable around the external surface of pipe i, and $\mathcal{T}_{1,j}$ the dimensionless temperature in a borehole-matrix system subject to a heat source at pipe j. Considering that the heat sources can be represented as point-heat-injections localized at the center of the pipes, $\mathcal{T}_{1,j}$ is equal to $\mathcal{T}_1$ defined in Section 2.2 with $(\rho^*, \theta^*) = (\rho_j, \theta_j)$ where (ρ_j, θ_j) is the position of the center of pipe j.

In a general manner, the latter integral can be evaluated numerically using expression (8a) to describe $\mathcal{T}_{1,j}$. A simplified expression can be deduced analytically by (i) describing $\mathcal{T}_{1,j}$ with the asymptotic expression (10); and (ii) considering a U-pipe localized at the borehole center. Considering the dimensionless asymptotic TRT temperature $\mathcal{T}_{TRT}^{\infty}$ defined as $\mathcal{T}_{TRT}^{\infty} = T_{TRT}^{\infty} K_1/Q$ with T_{TRT}^{∞} the asymptotic expression of (C.12), the resulting analytical expression is

$$\begin{aligned}\mathcal{T}_{TRT}^{\infty} &= \frac{1}{4\pi\kappa}\left[\ln(\tau) + \ln(4a) - \gamma\right] \\ &+ \frac{1}{4\pi}\left[-\ln\left(D_1\rho_{out}\right) + \frac{\kappa-1}{\kappa+1}\ln\left(D_2\right) + \frac{1}{\kappa_p}\ln\left(\frac{\rho_{out}}{\rho_{in}}\right)\right],\end{aligned} \tag{C.13}$$

where $\kappa_p = K_p/K_1$, $D_1 = s/R$ with s the distance between the two pipes, $D_2 = 1 - {D_1}^4/16$, and ρ_{in} and ρ_{out} are the dimensionless inner and outer radius of the pipes, respectively.

References

Abramowitz, M., and I. Stegun (1972), *Handbook of Mathematical Functions: With Formulas, Graphs, and Mathematical Tables*, Applied mathematics series, Dover Publications.

Al-Hadhrami, H., and M. Blunt (2001), Thermally induced wettability alteration to improve oil recovery in fractured reservoirs, *SPE Reservoir Evaluation and Engineering*, *4*(3), 179–186, 2000 SPE/DOE Improved Oil Recovery Symposium, Tulsa, Oklahoma, APR 03-05, 2000.

Anderson, M. P. (2005), Heat as a ground water tracer, *Ground Water*, *43*(6), 951–968, doi:10.1111/j.1745-6584.2005.00052.x.

Beck, A. E., F. M. Anglin, and J. H. Sass (1971), Analysis of heat flow data-in situ thermal conductivity measurements, *Canadian Journal of Earth Sciences*, *8*(1), 1–19, doi:10.1139/e71-001.

Bozzoli, F., G. Pagliarini, S. Rainieri, and L. Schiavi (2011), Estimation of soil and grout thermal properties through a TSPEP (two-step parameter estimation procedure) applied to TRT (thermal response test) data, *Energy*, *36*(2), 839–846, doi:10.1016/j.energy.2010.12.031.

Carslaw, H., and J. Jaeger (1986), *Conduction of Heat in Solids*, Oxford science publications, Clarendon Press.

Chen, X., and P. M. Shearer (2011), Comprehensive analysis of earthquake source spectra and swarms in the Salton Trough, California, *Journal of Geophysical Research-Solid Earth*, *116*, doi:10.1029/2011JB008263.

Ciocca, F., I. Lunati, N. Van de Giesen, and M. B. Parlange (2012), Heated Optical Fiber for Distributed Soil-Moisture Measurements: A Lysimeter Experiment, *Vadose Zone Journal*, *11*(4), doi:10.2136/vzj2011.0199.

Coleman, T. I., B. L. Parker, C. H. Maldaner, and M. J. Mondanos (2015), Groundwater flow characterization in a fractured bedrock aquifer using active DTS tests in sealed boreholes, *Journal of Hydrology*, *528*, 449–462, doi:10.1016/j.jhydrol.2015.06.061.

Conant, B. (2004), Delineating and quantifying ground water discharge zones using streambed temperatures, *Ground Water*, *42*(2), 243–257, doi:10.1111/j.1745-6584.2004.tb02671.x.

Constantz, J. (2008), Heat as a tracer to determine streambed water exchanges, *Water Resources Research*, *44*(4), W00D10, doi:10.1029/2008WR006996.

Eppelbaum, L. (2014), *Applied Geothermics*, Lecture notes in earth system sciences, Springer.

Esen, H., and M. Inalli (2009), In-situ thermal response test for ground source heat pump system in Elazig, Turkey, *Energy and Buildings*, *41*(4), 395–401, doi:10.1016/j.enbuild.2008.11.004.

Eskilson, P. (1987), *Thermal Analysis of Heat Extraction Boreholes*, Lund-MPh, Lund University Press.

Gelet, R., B. Loret, and N. Khalili (2012), A thermo-hydro-mechanical coupled model in local thermal non-equilibrium for fractured HDR reservoir with double porosity, *Journal of Geophysical Research: Solid Earth*, *117*(B7), doi:10.1029/2012JB009161.

Gunasekera, R., G. Foulger, and B. Julian (2003), Reservoir depletion at The Geysers geothermal area, California, shown by four-dimensional seismic tomography, *Journal of Geophysical Research-Solid Earth*, *108*(B3), doi:10.1029/2001JB000638.

Hu, P., Q. Meng, Q. Sun, N. Zhu, and C. Guan (2012), A method and case study of thermal response test with unstable heat rate, *Energy and Buildings*, *48*(0), 199–205, doi:10.1016/j.enbuild.2012.01.036.

Jorand, R., C. Vogt, G. Marquart, and C. Clauser (2013), Effective thermal conductivity of heterogeneous rocks from laboratory experiments and numerical modeling, *Journal of Geophysical Research: Solid Earth*, *118*(10), 5225–5235, doi:10.1002/jgrb.50373, 2013JB010166.

Klepikova, M. V., T. Le Borgne, O. Bour, and P. Davy (2011), A methodology for using borehole temperature-depth profiles under ambient, single and cross-borehole pumping conditions to estimate fracture hydraulic properties, *Journal of Hydrology*, *407*(1–4), 145–152, doi:10.1016/j.jhydrol.2011.07.018.

Klepikova, M. V., T. Le Borgne, O. Bour, K. Gallagher, R. Hochreutener, and N. Lavenant (2014), Passive temperature tomography experiments to characterize transmissivity and connectivity of preferential flow paths in fractured media, *Journal of Hydrology*, *512*(0), 549–562, doi:10.1016/j.jhydrol.2014.03.018.

Lamarche, L., and B. Beauchamp (2007a), A new contribution to the finite line-source model for geothermal boreholes, *Energy and Buildings*, *39*(2), 188–198, doi:10.1016/j.enbuild.2006.06.003.

Lamarche, L., and B. Beauchamp (2007b), New solutions for the short-time analysis of geothermal vertical boreholes, *International Journal of Heat and Mass Transfer*, *50*(7–8), 1408–1419, doi: 10.1016/j.ijheatmasstransfer.2006.09.007.

Lamarche, L., S. Kajl, and B. Beauchamp (2010), A review of methods to evaluate borehole thermal resistances in geothermal heat-pump systems, *Geothermics*, *39*(2), 187–200, doi:10.1016/j.geothermics.2010.03.003.

Lin, W. (2002), Permanent strain of thermal expansion and thermally induced microcracking in Inada granite, *Journal of Geophysical Research-Solid Earth*, *107*(B10), doi:10.1029/2001JB000648.

Lowry, C. S., J. F. Walker, R. J. Hunt, and M. P. Anderson (2007), Identifying spatial variability of groundwater discharge in a wetland stream using a distributed temperature sensor, *Water Resources Research*, *43*(10), W10,408, doi:10.1029/2007WR006145.

Pehme, P., B. Parker, J. Cherry, J. Molson, and J. Greenhouse (2013), Enhanced detection of hydraulically active fractures by temperature profiling in lined heated bedrock boreholes, *Journal of Hydrology*, *484*(0), 1–15, doi:10.1016/j.jhydrol.2012.12.048.

Pehme, P., B. L. Parker, J. A. Cherry, and D. Blohm (2014), Detailed measurement of the magnitude and orientation of thermal gradients in lined boreholes for characterizing groundwater flow in fractured rock, *Journal of Hydrology*, *513*(0), 101–114, doi:10.1016/j.jhydrol.2014.03.015.

Pehme, P. E., J. P. Greenhouse, and B. L. Parker (2007), The active line source temperature logging technique and its application in fractured rock hydrogeology, *Journal of Environmental & Engineering Geophysics*, *12*(4), 307–322, doi:10.2113/JEEG12.4.307.

Popov, Y. A., D. F. Pribnow, J. H. Sass, C. F. Williams, and H. Burkhardt (1999), Characterization of rock thermal conductivity by high-resolution optical scanning, *Geothermics*, *28*(2), 253–276, doi:10.1016/S0375-6505(99)00007-3.

Rainieri, S., F. Bozzoli, and G. Pagliarini (2011), Modeling approaches applied to the thermal response test: A critical review of the literature, *HVAC&R Research*, *17*(6), 977–990, doi:10.1080/10789669.2011.610282.

Raymond, J., and L. Lamarche (2014), Development and numerical validation of a novel thermal response test with a low power source, *Geothermics*, *51*, 434–444, doi:10.1016/j.geothermics.2014.02.004.

Raymond, J., R. Therrien, L. Gosselin, and R. Lefebvre (2011a), A review of thermal response test analysis using pumping test concepts, *Ground Water*, *49*(6), 932–945, doi:10.1111/j.1745-6584.2010.00791.x.

Raymond, J., R. Therrien, and L. Gosselin (2011b), Borehole temperature evolution during thermal response tests, *Geothermics*, *40*(1), 69–78, doi:10.1016/j.geothermics.2010.12.002.

Raymond, J., L. Lamarche, and M. Malo (2015), Field demonstration of a first thermal response test with a low power source, *Applied Energy*, *147*, 30–39, doi:10.1016/j.apenergy.2015.01.117.

Raymond, J., R. Therrien, L. Gosselin, and R. Lefebvre (2011), Numerical analysis of thermal response tests with a groundwater flow and heat transfer model, *Renewable Energy*, *36*(1), 315–324, doi: 10.1016/j.renene.2010.06.044.

Read, T., O. Bour, V. Bense, T. Le Borgne, P. Goderniaux, M. Klepikova, R. Hochreutener, N. Lavenant, and V. Boschero (2013), Characterizing groundwater flow and heat transport in fractured rock using fiber-optic distributed temperature sensing, *Geophysical Research Letters*, *40*(10), 2055–2059, doi:10.1002/grl.50397.

Read, T., O. Bour, J. S. Selker, V. F. Bense, T. L. Borgne, R. Hochreutener, and N. Lavenant (2014), Active-distributed temperature sensing to continuously quantify vertical flow in boreholes, *Water Resources Research*, *50*(5), 3706–3713, doi:10.1002/2014WR015273.

Regenstreif, E. (1977), On the Interior Dirichlet Problem of the Infinite Circular Cylinder: Green's Function for the Circular Cylinder, *Tech. rep.*, European Organization for Nuclear Research.

Roubinet, D., J.-R. de Dreuzy, and D. M. Tartakovsky (2012), Semi-analytical solutions for solute transport and exchange in fractured porous media, *Water Resources Research*, *48*(1), W01,542, doi: 10.1029/2011WR011168.

Roubinet, D., J. Irving, and F. D. Day-Lewis (2015), Development of a new semi-analytical model for cross-borehole flow experiments in fractured media, *Advances in Water Resources*, *76*(0), 97–108, doi: 10.1016/j.advwatres.2014.12.002.

Ruiz Martinez, A., D. Roubinet, and D. M. Tartakovsky (2014), Analytical models of heat conduction in fractured rocks, *Journal of Geophysical Research-Solid Earth*, *119*(1), 83–98, doi:10.1002/2012JB010016.

Saar, M. (2011), Review: Geothermal heat as a tracer of large-scale groundwater flow and as a means to determine permeability fields, *Hydrogeology Journal*, *19*(1), 31–52, doi:10.1007/s10040-010-0657-2.

Sharqawy, M. H., S. A. Said, E. M. Mokheimer, M. A. Habib, H. M. Badr, and N. A. Al-Shayea (2009), First in situ determination of the ground thermal conductivity for borehole heat exchanger applications in Saudi Arabia, *Renewable Energy*, *34*(10), 2218–2223, doi:10.1016/j.renene.2009.03.003.

Shen, P. Y., and A. E. Beck (1986), Stabilization of bottom hole temperature with finite circulation time and fluid flow, *Geophysical Journal of the Royal Astronomical Society*, *86*(1), 63–90, doi:10.1111/j.1365-246X.1986.tb01073.x.

Stehfest, H. (1970), Algorithm 368: Numerical inversion of laplace transform, *Communication of the ACM*, *13*(1), 47–49.

Wagner, R., and C. Clauser (2005), Evaluating thermal response tests using parameter estimation for thermal conductivity and thermal capacity, *Journal of Geophysics and Engineering*, *2*(4), 349–356, doi:10.1088/1742-2132/2/4/S08, International Workshop on New and Classical Applications of Heat Flow Studies, Aachen, GERMANY, OCT 04-07, 2004.

Wagner, V., T. Li, P. Bayer, C. Leven, P. Dietrich, and P. Blum (2014), Thermal tracer testing in a sedimentary aquifer: field experiment (Lauswiesen, Germany) and numerical simulation, *Hydrogeology Journal*, *22*(1), 175–187, doi:10.1007/s10040-013-1059-z.

Wang, H. F., B. P. Bonner, S. R. Carlson, B. J. Kowallis, and H. C. Heard (1989), Thermal stress cracking in granite, *Journal of Geophysical Research: Solid Earth*, *94*(B2), 1745–1758, doi:10.1029/JB094iB02p01745.

Wang, J. S. Y., C. F. Tsang, N. G. W. Cook, and P. A. Witherspoon (1981), A study of regional temperature and thermohydrologic effects of an underground repository for nuclear wastes in hard rock, *Journal of Geophysical Research: Solid Earth*, *86*(B5), 3759–3770, doi:10.1029/JB086iB05p03759.

Weiss, J. (2003), Using fiber optics to detect moisture intrusion into a landfill cap consisting of a vegetative soil barrier, *Journal of the Air and Waste Management Association*, *53*(9), 1130–1148.

Xiang, Y., and Y. Zhang (2012), Two-Dimensional Integral Equation Solution of Advective-Conductive Heat Transfer in Sparsely Fractured Water-Saturated Rocks with Heat Source, *International Journal of Geomechanics*, *12*(2), 168–175, doi:10.1061/(ASCE)GM.1943-5622.0000109.

Zheng, X., L. Zhang, Q. Ren, and H. Qian (2013), A thermal response method of calculating a soil's thermal properties when backfill material information is unavailable, *Energy and Buildings*, *56*(0), 146–149, doi: 10.1016/j.enbuild.2012.09.020.